

Model-based and model-free characterization of epidemic outbreaks — Technical notes on Dehning et al., Science, 2020

Jonas Dehning¹, F. Paul Spitzner¹, Matthias Linden², Sebastian B. Mohr^{1,3}, Joao Pinheiro Neto¹, Johannes Zierenberg¹, Michael Wibral⁴, Michael Wilczek^{1,5}, and Viola Priesemann^{1,5,6}

¹ *Max Planck Institute for Dynamics and Self-Organization, Am Fassberg 17, 37077 Göttingen.*

² *Institute for Theoretical Physics, Leibniz University, 30167 Hannover, Germany.*

³ *Institute for Theoretical Physics, University Leipzig, Postfach 100 920, 04009 Leipzig, Germany.*

⁴ *Campus Institute for Dynamics of Biological Networks, University of Göttingen, Hermann-Rein-Straße 3, 37075 Göttingen, Germany.*

⁵ *Institute for the Dynamics of Complex Systems, University of Göttingen, Friedrich-Hund-Platz 1, 37077 Göttingen, Germany.*

⁶ *Bernstein Center for Computational Neuroscience, Hermann-Rein-Str. 3, 37075 Göttingen, Germany.*

(Dated: June 22, 2020)

In this technical note, we provide additional background on our Bayesian inference for change-point detection in COVID-19 case numbers (Dehning et al., Science, 2020). In particular, we explore basic properties of model-based and model-free estimates of the reproduction number, discuss what conclusions can be drawn from Bayesian analyses, further develop our model and apply it to newly available data, and discuss potential issues with changes in testing policies.

This technical note presents work in progress and should be considered like an internal draft. It is not ready for submission yet, and is being frequently updated.

CONTENTS

		43	VI. Behavioral changes and interpretation of results.	16
		44		
14	I. Introduction	1		
		45	VII. Summary & Conclusions	16
15	II. Estimating the reproductive number	2		
	A. Basic SIR dynamics	2	References	16
16				
17	B. Model-free estimation of reproduction number R_t	3	VIII. Supplementary Information: Figures	17
18				
19	C. Model-free methods versus model-based methods to infer reproductive number.	6		
20				
		48	I. INTRODUCTION	
21	III. What conclusions can one draw from a Bayesian analysis?	7		
22				
23	A. Modeling background	7		
24	B. Bayesian inference as reasoning under uncertainty, bound to be updated	8		
25				
26	C. Conditions for plausible alternative models entering model comparison	8		
27				
28	D. Models as competing causal explanations of data	8		
29				
30	IV. Model evolution	9		
31				
32	A. Model updates based on time of symptom onset and comparison to previous results based on time of reporting	9		
33				
34	B. Differences between results based on RKI versus JHU data sources	10		
35				
36	V. Impact of Testing	10		
37				
38	A. Strong growth of new cases until week 12	11		
39	B. The reporting delay relates reported cases to disease dynamics	11		
40	C. Decomposing the epi curve into weeks of testing	13		
41				
42	D. Available data on testing	15		

After the initial release of our manuscript "Inferring change points in the spread of COVID-19 reveals the effectiveness of interventions" in Science [1], we have received many constructive comments and interesting questions, and have also faced some recurring misunderstandings. This technical note is intended to answer the most important of these questions, to give additional background for understanding our results, and to also discuss the robustness and performance of our model in the light of newly available data, in particular data based on symptom onset times.

The inspiration and comments we received can be broadly categorized into four topics:

1. Remarks on apparent discrepancies between the values for the estimated reproductive number \hat{R} as reported by the Robert Koch Institute (RKI) and the corresponding spreading rate resulting from our published analysis. We will explain below how this apparent discrepancy partly arises from the comparison of model-free estimates to those from a differential-equation based modeling of disease dynamics. We show how the model-free approach may substantially underestimate the reproductive number R immediately after a sudden drop in R has occurred. From the comments we received it seems

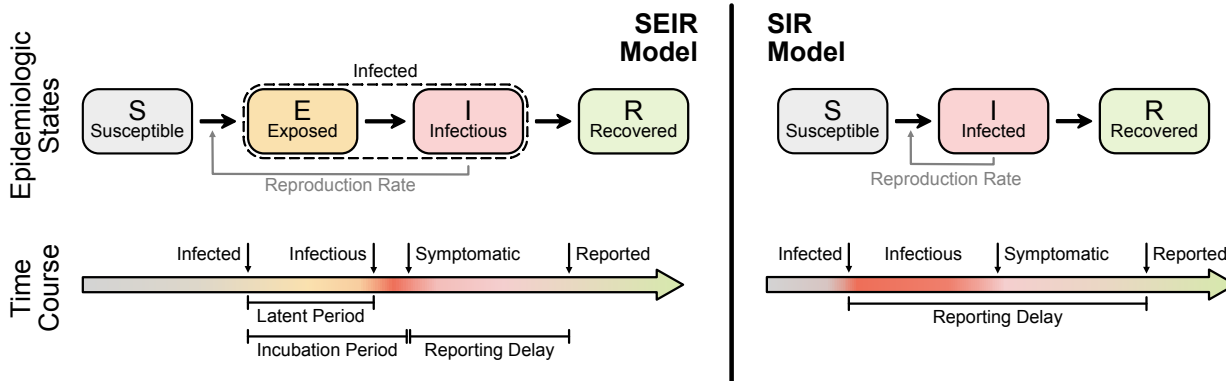


FIG. 1. **Illustration of two basic compartmental models in epidemiology.** The SEIR model (left) captures the basic steps that infections passes through: A healthy person becomes infected but not infectious (leaves S, enters E); after some time (‘latent period’) the person becomes infectious (leaves E, enters I) but symptoms only show after some incubation period; after some time the person is no longer infectious (leaves I, enters R), which can have several reasons including isolation, conventional recovery, or death. The SIR model (right) is the most basic compartmental model and does not distinguish between infectious and infected: A healthy person becomes infected (leaves S, enters I), immediately begins to infect other persons but only shows symptoms with a delay. After some time the person “recovers” (leaves I, enters R), which again includes isolation, recovery, or death.

74 that this very important fact related to estimating 107
 75 R , i.e. \hat{R} , is largely unknown, and also counter- 108
 76 intuitive to most readers. This effect, together with 109
 77 the usage of alternative data (see point 3.), explains 110
 78 the apparent discrepancies between the RKI reports 111
 79 and our study. We therefore derive and demonstrate 112
 80 it in detail here. 113

81 2. Questions revolving around the philosophy and inter- 114
 82 pretation of our modeling approach that combines a 115
 83 differential equation model of the disease outbreak, 116
 84 Bayesian parameter inference and Bayesian model 117
 85 comparison. Most frequently we were asked if and 118
 86 in what sense our results have a causal interpreta- 119
 87 tion. As we will explain below, our approach selects 120
 88 the most plausible of multiple causal explanations 121
 89 of the observed data, but does not establish strict 122
 90 interventional causality. 123

91 3. New data have been released in the time since our 124
 92 analyses were completed. Most prominently, data 125
 93 on the times of symptom onsets (epi curve) are 126
 94 now accessible. The advantage is that the date of 127
 95 symptom onsets is closer to the infection date, al- 128
 96 lowing in principle a more precise estimation of the 129
 97 dynamics of the propagation. It brings however its 130
 98 own source of errors, because the onset of symp- 131
 99 toms is not reported for all cases. As we will show 132
 100 below, our central conclusions remain unchanged 133
 101 when updating our model to the new data. 134

102 4. Questions on how changes in testing capacity may 135
 103 have influenced our results. Given the data that 136
 104 have become available on the weekly (daily) number 137
 105 of performed tests, test capacity, and on delays 138
 106 between symptom onset, test and case report, we 139

reanalyze in great detail the disease and testing 140
 dynamics, especially with respect to the timing of 141
 the peak in new symptom onsets. We conclude that 142
 all symptom onsets that are relevant for the main 143
 conclusions of our previous publication have been 144
 tested at a time when testing had sufficient capacity 145
 and was sufficiently constant. 146

We will in the following address the issues revolving 147
 around the reproductive number R first, also introduc- 148
 ing the basic terminology of disease spreading and the 149
 fundamental difference between model-free and model- 150
 based estimation of epidemiological parameters. Next, we 151
 will discuss philosophy and interpretation of model-based 152
 estimation in the Bayesian framework and the causality 153
 question. We then show how our original analyses can be 154
 evolved to incorporate new data, in particular on symp- 155
 tom onset (epi curve). Last we turn to the important 156
 question of testing. 157

II. ESTIMATING THE REPRODUCTIVE NUMBER

A. Basic SIR dynamics

128 Before we define the reproductive number R , we briefly 129
 129 recapitulate the basic SIR dynamics that we consider 130
 130 (Fig. 1). In principle, the course of an infection can be 131
 131 described as follows: A susceptible person (not infected 132
 132 and not immune) becomes infected but is initially not 133
 133 infectious; after some time, the person starts to be in- 134
 134 fectious but symptoms only show after the incubation 135
 135 period; eventually, the person is no longer infectious be- 136
 136 cause she or he has been either isolated, has recovered, or

137 died. The idea of compartmental models is to group the
 138 population into compartments; in the most simple but
 139 established SIR model these are susceptible (S), infected
 140 (I), and recovered (R). Assuming a well-mixed population
 141 (a mean-field approximation of everybody interacting with
 142 everybody), one can formulate differential equations that
 143 describe the time development of these compartments:

$$\frac{dS}{dt} = -\lambda \frac{SI}{N} \quad (1)$$

$$\frac{dI}{dt} = \lambda \frac{SI}{N} - \mu I \quad (2)$$

$$\frac{dR}{dt} = \mu I \quad (3)$$

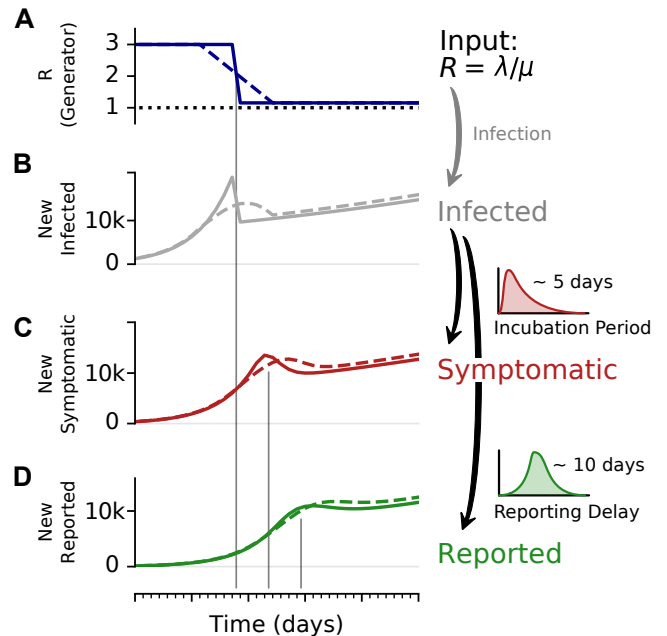
144 This assumes a spreading rate λ for infected people to
 145 infect susceptible people (who they meet randomly) and
 146 a recovery rate μ for infected people to recover. These
 147 differential equations can be extended to include various
 148 different compartments, in order to better resolve the
 149 temporal course of the disease, but typically keep the
 150 mean-field assumption of a well-mixed population unless
 151 evaluated on some (typically unknown) network. In this
 152 case, additional compartments reflect spatial information.

153 **Observed case numbers are always delayed from**
 154 **the true infection date (Fig. 2).** In general, when
 155 a person becomes infected, the onset of symptoms is
 156 delayed by the incubation period. Upon symptom onset, it
 157 typically takes a few days until the person undergoes a test
 158 and the case is reported (although some people are tested
 159 before symptom onset, e.g. if contacts are traced or tests
 160 are performed at random “Stichprobe”). However, for
 161 the modeling, one is usually interested in the actual time
 162 when a person becomes infected — but this information
 163 is not directly available in real-world data. One either
 164 works with the reporting date or with the dates of the
 165 symptom onset (epi curve) that can be reconstructed
 166 e.g. via questionnaires and imputation methods. Note that
 167 even symptom onset dates are still delayed with respect
 168 to the true infection dates due to the incubation period.
 169 For the reporting dates a second delay occurs between
 170 symptom onset and report, unless an asymptomatic case
 171 is discovered in random testing. For the example models
 172 in the following, we synthetically generate observed cases
 173 — symptomatic or reported — by convolving the infected
 174 cases with a distribution of incubation periods or reporting
 175 delays, respectively (Fig. 2).

176 B. Model-free estimation of reproduction number

$$177 R_t$$

178 **Definition of R .** The reproductive number R quanti-
 179 fies how many susceptible persons are on average infected
 180 by one infected person. If one infected person infects
 181 on average more than one other person ($R > 1$), then
 182 case numbers are growing exponentially. In contrast, if
 183 less than one other person gets infected ($R < 1$), then



184 **FIG. 2. A change-point in R can lead to a transient**
 185 **decrease in case numbers.** To illustrate the effect of a
 186 change point, and the delays in observing symptomatic and
 187 reported cases, we consider an SIR model with a fast or slow
 188 decrease of R , and generate synthetic case numbers. **A:** The
 189 reproductive number R exhibits a change point from $R = 3$
 190 to $R = 1.15$, with a duration of either 1 day (solid) or 9 days
 191 (dashed). **B:** The number of new infections can show a tran-
 192 sient decrease caused by the change point in R , even though
 193 the underlying dynamics are always in the exponentially grow-
 194 ing regime of $R > 1$. Such a decrease can be misinterpreted as
 195 $R < 1$. The number of **C** new symptomatic cases, and **D**
 196 reported cases is generated by convolving the new infected
 197 with a log-normal incubation period (median 5 days) or re-
 198 porting delay (median 10 days), respectively. Note that the
 199 convolution shifts and smooths the curve of the new infected.
 200 Nonetheless, the counter-intuitive effects of a transient de-
 201 crease in case numbers caused by a change point, is still very
 202 well visible (See Fig. 4 for the challenges in estimating R
 203 around the change point.)

184 case numbers are declining. Therefore, $R = 1$ marks
 185 the critical transition between growth and decline of case
 186 numbers. Last, note that $R \approx 1$ means that new infec-
 187 tions keep occurring at their current levels (which may be
 188 high, depending on when and how $R \approx 1$ was reached).

189 Estimating the reproductive number R in principle
 190 can be done in two manners, either by inferring it from
 191 observed case numbers, or by following infection chains
 192 step by step (which is not discussed here). If one infers
 193 it from observed case numbers, there are a number of
 194 possible approaches. Some approaches are summarized
 195 in Fig. 4 and detailed below. All of these approaches can
 196 be applied to the epi curve (day of symptom onset) or to

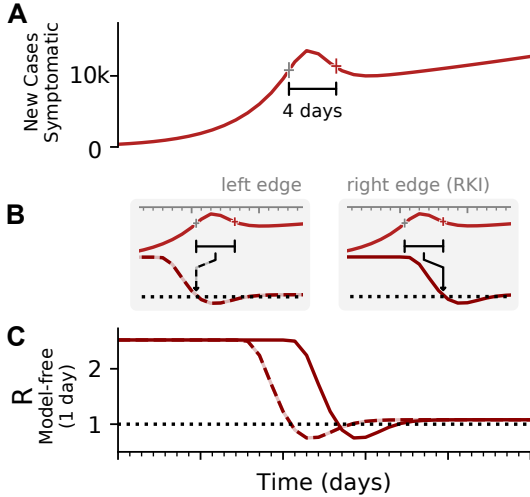


FIG. 3. **Two different conventions to define the reproductive number R : Infections in the future or infections from the past.** **A:** Synthetic data for new symptomatic cases. The marked interval indicates an assumed generation time of 4 days. **B:** The basic reproductive number can be defined either on the left edge of the generation interval (left, dashed line), describing the average number of future infections that are cause at time t , or on the right edge of the interval (right, solid line), describing the average number of infections at time t that were caused by the past ones. **C:** Depending on the convention, the resulting curve of R is shifted by the generation time g . Note that in both cases the R is estimated erroneously to fall below $R = 1$, although in the underlying model it was $R > 1$ all the time. This is an effect of the SIR dynamics together with a change point in the underlying R . (See Fig. 4 for model details, and Figs. - for other parameters).

197 the reported cases (day or reporting). In the following,
198 we assume that they are applied to the epi curve.

199 The most straight-forward definition of the reproductive
200 number assumes a reproductive process with offspring
201 generation, such as a branching process [2]. For this,
202 one assumes a generation time g in which an infectious
203 person can generate offspring infections. In the simplest
204 case, one could consider that offspring infections occur
205 exactly after one generation time g . This allows to infer
206 the reproductive number R precisely:

$$\hat{R}_t = \frac{\text{number of newly infected at time } t + g}{\text{number of newly infected at time } t} \quad (4)$$

$$= \frac{C_{t+g}}{C_t}. \quad (5)$$

207 In reality, these newly infected case numbers C_t have to
208 be approximated, e.g., by using new symptomatic cases
209 or new reported cases. Moreover, the generation times g
210 of each infection are widely distributed, so that using the
211 average value g (or an estimate of it) is used as a further
212 approximation.

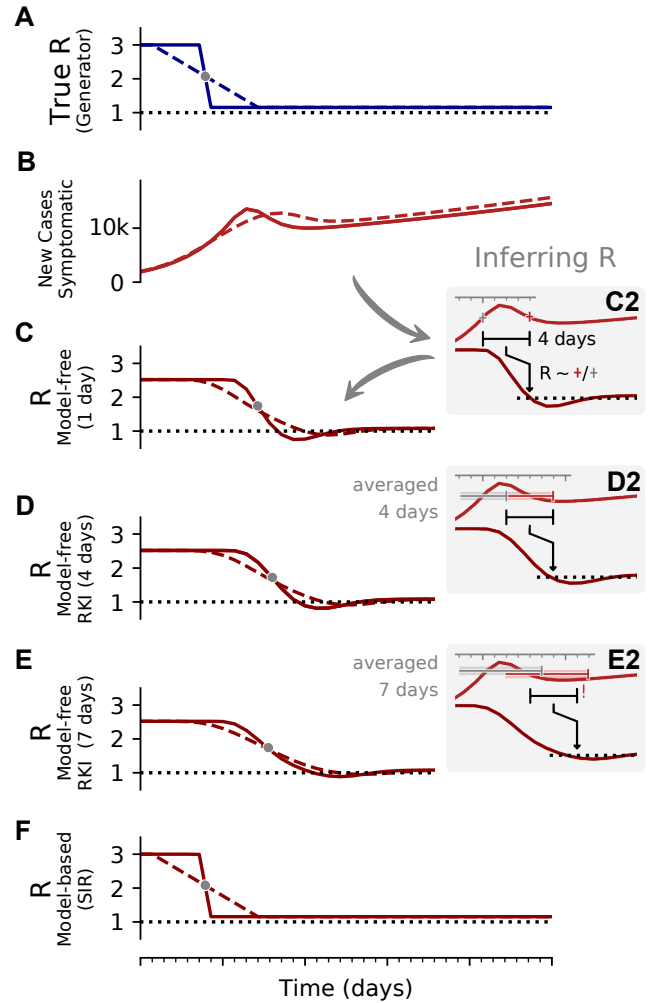


FIG. 4. **The inferred reproductive number \hat{R} depends on the inference method.** **A, B:** Synthetic data for new symptomatic cases generated with SIR dynamics from an underlying R with one change point of duration 1 day (solid) or 9 days (dashed). **C:** Model-free inference of \hat{R} based on the ratio of case numbers at time t and time $t - g$, marked by a red and gray cross (inset), respectively ('right-edge convention', cf. Fig. 3). **D:** Model-free inference of \hat{R} following the Robert Koch Institute convention, i.e. using the definition of C but with averaging over a window of the past 4 days (inset, red and gray bars). **E:** Same as D but averaging over 7 days. Note the overlap of intervals. All the model-free methods (C-E) can show an erroneous estimate of $R < 1$ transiently, due to the change point in the underlying true R . **F:** The inferred \hat{R} using change-point detection with an underlying dynamic model (SIR) does *not* show a transient erroneous $R < 1$ period. If the underlying dynamic model corresponds well enough to the true disease dynamics, then this approach reproduces the true R that was used to generate the data.

213 When going into detail, there are two different conven-
214 tions for the timing of the estimated reproductive number
215 \hat{R} with respect to the case numbers C_t (Fig. 3). Above, we
216 consider \hat{R}_t to characterize the number of future infections

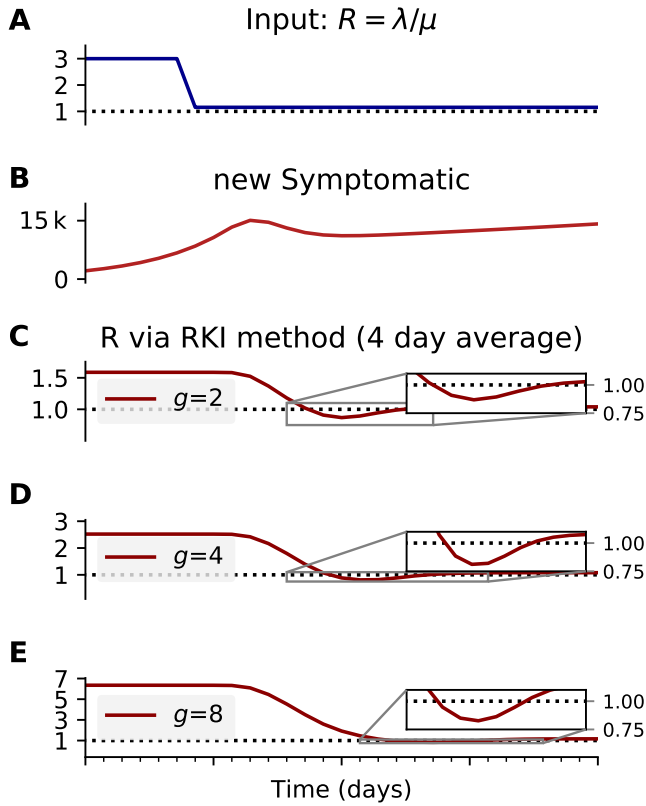


FIG. 5. **The inferred reproductive number depends on the assumed generation time g .** **A, B:** We generate synthetic data using SIR dynamics with time-dependent R including a 1-day change point (A) that yields new symptomatic cases with transient decrease (B) despite all $R > 1$. **C–E:** Using the RKI convention to infer \hat{R} (4-day average, right-edge convention), we demonstrate how generation times g result in different \hat{R} curves. In particular, we find different initial levels of R (left plateau), differently long crossover duration (time from left plateau to right plateau), and differently deep transients of $R < 1$ (insets).

217 that are caused by infections at time t (left-edge conven-
 218 tion). Alternatively, one can consider \hat{R}_t to characterize
 219 the number of infections at time t that were caused by
 220 the past pool of infected (right-edge convention), defined
 221 as

$$\hat{R}_t = \frac{\text{number of newly infected at time } t}{\text{number of newly infected at time } t - g} \quad (6)$$

$$= \frac{C_t}{C_{t-g}} \quad (7)$$

222 The results for \hat{R} are exactly equivalent, apart from
 223 a shift in time by exactly g . However, the distinction
 224 between left-edge and right-edge convention and the asso-
 225 ciated time-shift crucially matter when discussing changes
 226 in R_t with respect to interventions.

\hat{R} as calculated by the RKI. Real-world data are often noisy, and therefore averaging over a certain time

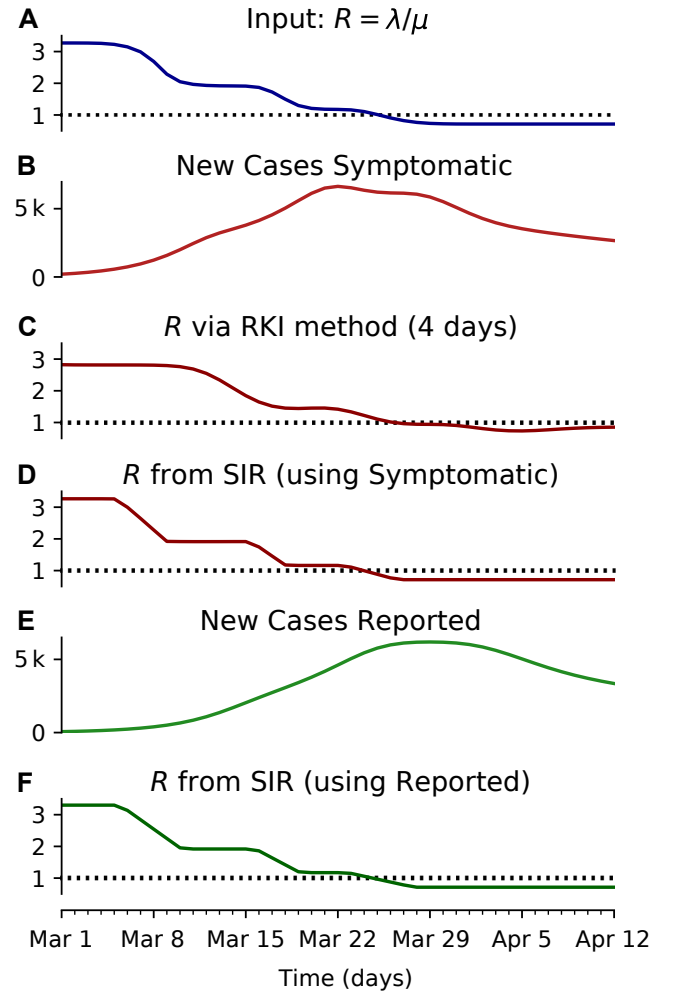


FIG. 6. **The model-based methodology yields consistent results irrespective of whether it is applied to the new reported cases or the new symptomatic cases** (e.g. obtained by nowcasting). **A:** Time-dependent reproductive number as inferred from case numbers in Germany [1]. **B:** Synthetic data for new symptomatic cases generated with SIR dynamics from the underlying time-dependent R . **C:** Inferred \hat{R} from new symptomatic cases using RKI method (4 days generation time, right-edge convention) would reproduce step-like behavior (no noise present) but drops below $R = 1$ (dotted line) already after the second change point (note that curve is shifted and smoothed compared to input R , cf. Fig. 4). **D:** Inferred \hat{R} from new symptomatic cases using change-point detection with dynamic model (SIR) correctly reproduces the input. **E:** Synthetic data for new reported cases generate with SIR dynamics as in B (cf. Fig. 2). **F:** Inferred \hat{R} from new reported cases (E) using change-point detection with dynamic model (SIR) also correctly reproduces the input. Note that both, D and F show sharper steps because of the assumed piece-wise linear change points in the model, and that they perform so well because they employ the true dynamic model that is used for the synthetic data. Both are model assumptions that need to be justified in our approach.

window can help to smooth the estimate. This procedure

is used in two variants by the RKI, smoothing over four days or over seven days. The details of the procedure are documented in detail in Ref. [3]. For both smoothing lengths, they assume a constant serial interval (generation time) of $g = 4$ days (Fig. 4) and the right-edge convention. The four-day smoothing has the advantage that it reacts a bit faster, the seven-day smoothing has the advantage that it smooths better the relatively strong variations. In particular,

$$\hat{R}_{t,4} = \frac{\sum_{s=t-3}^t C_s}{\sum_{s=t-3}^t C_{s-g}} \quad (8)$$

$$\hat{R}_{t-1,7} = \frac{\sum_{s=t-6}^t C_s}{\sum_{s=t-6}^t C_{s-g}}, \quad (9)$$

where $g = 4$ is the assumed generation duration, and the averaging is done over 4 and 7 days, respectively. Note the shift by one day in the 7-day version Eq. (9).

Model-free methods also build on assumptions. Clearly, when using *model-based* methods, assumptions go into the model itself; but also when using what we call *model-free* methods, assumptions have to be made. In particular, the core assumptions behind the model-free approach to estimate R that we discussed so far are that every new infected person infects on average R persons, and it does so precisely g days after becoming infected. As is the case in modelling, these assumptions present a simplification of the complex real-world dynamics. Whether a chosen way to answer a given question is reasonable or not depends on the specific question one asks (every question may need its own model simplifications and type of data set), on the quality of the data, and on how well the *relevant* real-world dynamics for the question are captured in the simplified model. For the question of whether case numbers are increasing or decreasing *in general*, the above method of calculating R has proven very useful.

C. Model-free methods versus model-based methods to infer reproductive number.

In order to demonstrate potential issues when inferring the reproductive number R , we systematically compare the model-free methods with model-based methods (akin to our analysis of λ^* in [1]) on synthetic data from an SIR model (Fig. 2). With model-free methods, we refer to inference methods for R , which do not explicitly incorporate disease dynamics (SIR). The three methods we presented above belong to this group. These methods to estimate R are straight forward and easy to implement. However, they might lead to biased estimates when R is changing rapidly. More precisely, in the following we show that these methods (1) smooth out fast changes in R , (2) produce some delay compared to the underlying R , (3) the estimate depends on the assumed generation time, and (4) around change points they may return transiently $R < 1$, even if the true value was never smaller than 1.

While these methods have the above limitations when R is changing quickly, they are still very useful for an easy-to-obtain estimate of R .

1. Model-free methods may smooth out fast changes.

In Fig. 4, the \hat{R} that is inferred by model-free methods undergoes a smoother change than the true R . The smoothing has two origins: First, when using the sliding-window of four or seven days (RKI methods), multiple days are combined to obtain an \hat{R} value for one day. Second, \hat{R} has to be calculated from the daily new symptomatic or reported cases (Fig. 2 C, D), because the dates of infection (Fig. 2 B) are not directly accessible in real-world data. As discussed before, symptom onset and reporting date are delayed from the infection date. Because the delays vary from case-to-case, these two curves are smoothed out compared to the infection curve (in other words, the smoothing originates from the variance in incubation period and reporting delay, see later Fig. 10 in the section about testing). Hence, if smoothing is not explicitly incorporated in the inference of R , fast changes appear slower than they truly are, and successive fast changes may appear as a long transient.

2. Model-free methods produce delayed estimates that are difficult to interpret

In our example in Fig. 4, we estimated \hat{R} based on the number of new symptomatic cases as produced by our synthetic disease model. The \hat{R} of all three model-free methods is shifted in time compared to the true R (Fig. 4 A).

How does one interpret the shift and where does it come from? To interpret the shift and compare between the different methods, we focus on the time point where half of the steep step in R has been detected (gray dots). This shift has multiple contributions. One contribution originates from using the dates of symptom onset, which is shifted on average by the incubation period (in our example ≈ 5 days). This generates the 4–5 day shift of the one-day method (Fig. 4 C). Because the incubation period is not constant and typically asymmetric, there is an additional asymmetric distortion towards either direction, depending on the shape of the actual distribution of incubation periods. Another source for the shift comes from the time average, which explains the additional (approximate) 1–2 day shift in the four-day and seven-day methods employed by the RKI (Fig. 4 D, E). Because of the specific definition of the position of the 4 and 7-day window of the RKI (see eq. 8, 9), the two versions of \hat{R} have a very similar average average delay of 5–6 days in total with respect to the true R .

Both, the variable incubation time and the time averaging also impact the start- and end-points of the change in a non-trivial manner. In combination, multiple sources

318 cause shifts that can point into opposite directions. While
 319 the sources can be identified conceptually, the combined
 320 effect cannot be perfectly disentangled or compensated.

321 Due to multiple sources of shifts and smoothing, a
 322 simple post-hoc shift of the \hat{R} -curve cannot reproduce the
 323 true R around a change point. For example, a shift of
 324 Fig. 4D by 5 days would suggest a start of the change point
 325 before it starts in reality (Fig. 4 A). This fact has led to
 326 multiple prominent misunderstandings in relation to the
 327 RKI data and the effects of governmental interventions.
 328 Instead of shifting curves to partially correct for one or
 329 another potential delay, an inference of R using model-
 330 based methods can account for this and other potential
 331 biases. When using a good model, such a model-based
 332 approach returns the correct R with the correct steepness
 333 and time point (Fig. 4 E, for technical details, see Methods
 334 in [1]).

335 3. R -estimates depend on the assumed generation time.

336 The assumed generation time g impacts the magnitude
 337 of the estimated reproductive number \hat{R} (Fig. 5). We
 338 exemplify this effect using the method of the RKI (4-day
 339 average), where we vary the assumed (constant) gener-
 340 ation time g . In particular, the chosen generation time
 341 ($g = 2, 4$ or 8) affects the initial plateau ($\hat{R} \simeq 1.6, 2.5$ and
 342 6.4 respectively), the duration of the inferred change, and
 343 the depth of the transient underestimation. This small
 344 example shows that estimating the magnitude of the re-
 345 productive number from observed case numbers without
 346 knowing the precise generation time can be challenging.

347 4. Model-free methods may return erroneous transient 348 periods of $R < 1$ at change points.

349 In our examples (Figs. 4 and 5), we consider that R
 350 changes rapidly from $R_0 = 3$ to $R_1 = 1.15$ within one day
 351 (full lines). Such a sudden change leads to a transient
 352 decrease in new case numbers — despite R being always
 353 > 1 . How can there be decrease in new cases although
 354 $R > 1$? The transient decrease results from the pool of
 355 infected suddenly infecting considerably less people. This
 356 decrease in infections causes the sharp peak and a sudden
 357 drop in new infections (Fig. 2 B, solid line). It then
 358 carries over to the number of new symptomatic and new
 359 reported cases, with the respective delay and smoothing
 360 (Fig. 2 C, D). This transient decrease depends on the
 361 duration of the change point: While it is strongest for
 362 steep changes, it also occurs for a change point with a
 363 transient time of nine days (Fig. 2, dashed line).

364 Naively, a transient decrease might be interpreted as
 365 a transient $R < 1$, but that is not the case here. A
 366 model-free method cannot distinguish between different
 367 causes for transient decreases in case numbers, being it
 368 due to transient non-linear effects (Fig. 2) or due to a
 369 true exponential decay ($R < 1$). The model-free meth-

370 ods in our example (Figs. 4 and 5) correspondingly yield
 371 non-negligible periods of $R < 1$, even though the under-
 372 lying model dynamics have $R > 1$ always. Model-based
 373 approaches, on the other hand, can account for transient
 374 non-linear effects if included in the model, e.g., as change
 375 points, and — if the model is correct — even reproduce
 376 the true underlying dynamics (Fig. 4 F). To conclude,
 377 if one infers R in a model-free manner, by computing
 378 ratios of case numbers, one interprets reductions in case
 379 numbers as $\hat{R} < 1$ (Fig. 4 C–E). After strong decreases
 380 of the true R this may be an incorrect interpretation.

381 5. Well chosen model-based methods can reconstruct 382 complex disease dynamics

383 When the chosen model describes the true disease dy-
 384 namics well, robust inference of the true underlying repro-
 385 duction number (and other parameters) is possible. To
 386 demonstrate the robustness of model-based inference, we
 387 generate synthetic data using an SIR-model as inferred
 388 from case numbers in Germany between March 2 and
 389 April 21 [1] (Fig. 6). The Bayesian model inference can
 390 recover the reproductive rate (Fig. 6 D, F), whereas with
 391 the model-free method, the recovered R is slightly biased
 392 (Fig. 6 C). Note, however, that the chosen model has to
 393 match at least approximately the disease dynamics, to
 394 allow a good inference. This is why we used different
 395 models to assess the robustness of our results in Ref. [1]
 396 (SIR: Fig. 3, SEIR-like: Fig. S3, SIR without weekend
 397 modulation: Fig. S4).

398 III. WHAT CONCLUSIONS CAN ONE DRAW 399 FROM A BAYESIAN ANALYSIS?

400 A. Modeling background

401 When the Coronavirus-pandemic arrived in Germany
 402 we set out to model the spread of the disease as rapidly as
 403 possible. Thus, our model from the start was aimed at giv-
 404 ing estimates with their corresponding error bounds based
 405 on the data available at that time. To this end we decided
 406 to use a Bayesian strategy as it allowed formulating well-
 407 documented assumptions on those aspects not available
 408 from data at that time. Within the Bayesian framework
 409 these assumptions can and should be replaced by data
 410 as soon as these become available, and we implement
 411 such an improvement below for the case of information on
 412 symptom onset times that have become available in the
 413 meantime. Given such new data it will also be interesting
 414 to evaluate post-hoc the assumptions and the performance
 415 of our model. This will also give some guidance as to
 416 whether to employ a model of this kind again in a new sce-
 417 nario (another disease outbreak or pandemic) where some
 418 relevant data will also not be available immediately. We
 419 note that taking these steps is the intended development
 420 in Bayesian inference.

421 We also note that all statistical procedures come with
 422 their own assumptions, e.g. on distribution of the data,
 423 models of measurements and random errors. Bayesian
 424 analysis is no exception to this rule; in our view the only
 425 difference is that modeling assumptions are not taken for
 426 granted based on the long-established use of a method
 427 (say, a t-test) but need to be formulated anew for each
 428 case. The fact that the assumptions are hand-tailored to
 429 the application case may seem subjective sometimes; yet,
 430 similar assumptions are being made, more tacitly perhaps,
 431 in other frameworks, as well. This said, it is neverthe-
 432 less important to question and discuss (our) modeling
 433 assumptions and to test the sensitivity of our results to
 434 these modeling assumptions. We have already concisely
 435 discussed our assumptions in the main manuscript [1], but
 436 we here give a much deeper, broader and more educational
 437 treatment.

438 B. Bayesian inference as reasoning under 439 uncertainty, bound to be updated

440 The results of a Bayesian analysis at some publication
 441 time point T represent what we should consider most
 442 plausible at that time point T , given the knowledge avail-
 443 able at T (causes and data known at T). These results
 444 represent something that we should be able to agree on
 445 given the knowledge at T (and some practical constraints,
 446 see below), but these results may change given more infor-
 447 mation at a later time $T + \Delta T$. Changing one’s mind with
 448 the availability of additional information is designed into
 449 Bayesian inference as “the logic of science” (E.T. Jaynes,
 450 [4]) from the start. In other words, scientific inference
 451 and the associated models are bound to be updated. The
 452 important question is thus not whether a model is correct
 453 in absolute terms, but whether it was possible to agree
 454 on the model (and the inference provided by it) at time
 455 T , and also if the inference provided at T was robust,
 456 for example in the sense that the credible intervals for
 457 the model parameters at T comprise those obtained at
 458 $T + \Delta T$.

459 From this perspective, it is obvious that now, more
 460 than a month after finalization of our published analyses
 461 on April 21, new data have become available and that
 462 the model can, and should, be improved accordingly. Im-
 463 portant data in this respect are data on reconstructed
 464 infection dates which at present take about 7 days to come
 465 in for at last 80% of the cases (Fig. 10), and took even
 466 longer during the early stages of the outbreak. We present
 467 results obtained using these data below and compare them
 468 to our published results.

469 C. Conditions for plausible alternative models 470 entering model comparison

471 A frequent, and important misunderstanding around
 472 Bayesian model comparison is that one is allowed to

473 formulate very many models at random and then let the
 474 data decide on the best model via the Bayesian model
 475 evidence (or the LOO-scores). This notion fails to notice
 476 that the model evidence $p(D|M_i)$ is only one part of the
 477 decision on the preferred model. The formal equation for
 478 deciding between models i and j would be:

$$\frac{p(M_i|D)}{p(M_j|D)} = \frac{p(D|M_i) p(M_i)}{p(D|M_j) p(M_j)}, \quad (10)$$

479 i.e. taking such a decision entails accounting for a-priori
 480 plausibility of different models, i.e. $p(M_i)$ and $p(M_j)$.
 481 While it is customary to assign equal a-priori plausibility
 482 to all the models being considered, this does not mean that
 483 just any model qualifies for use in this decision procedure.
 484 Rather, each model subjected to a model comparison
 485 needs to be well justified. This is one of the reasons why we
 486 did not consider for example models of sustained, constant
 487 drifts in the effective spreading rate λ^* (or, equivalently
 488 the reproductive number R), as we did not come up
 489 with plausible explanations for such a behavior (except
 490 perhaps arguments based on herd-immunity, which seem
 491 implausible now, in the light of second waves of infections
 492 and a recent rise in λ^* from its all-time low, and also in
 493 the light of country to country comparisons, Fig. 7).

494 On a practical note, useful modeling also has to reflect
 495 certain limits on model complexity in relation to the
 496 available data, and also computational resources. Known
 497 phenomena, that can nevertheless not be modeled must
 498 therefore often be integrated into noise terms that are
 499 designed accordingly (as was done with the modeling
 500 of observation noise in our case, instead of using full
 501 stochastic differential equations). The best that can be
 502 done then is to investigate the sensitivity of results with
 503 respect to the simplifying assumptions that have been
 504 made.

505 It is also in order to explain in simple terms how results
 506 of a Bayesian analysis may be interpreted: In the Bayesian
 507 framework probabilities are measures of the plausibility of
 508 statements about the world, given our present knowledge
 509 (see [4] for the exact mathematical derivation of this
 510 statement). Thus, the results of Bayesian parameter
 511 inference indicate credible (plausible) ranges in which we
 512 should assume the unknown parameters to be. Assuming
 513 them to be elsewhere with high probability would be
 514 inconsistent with the information we have. In this sense,
 515 these credible intervals may form the basis for decisions
 516 we have to take.

517 D. Models as competing causal explanations of 518 data

519 Last, we note that the notion of causality resides only
 520 in the construction of the models — with different models
 521 incorporating different possible causal explanations of the
 522 data (e.g. in the form of differential equations for the
 523 disease dynamics). Performing model comparisons then
 524 selects more plausible over less plausible explanations but

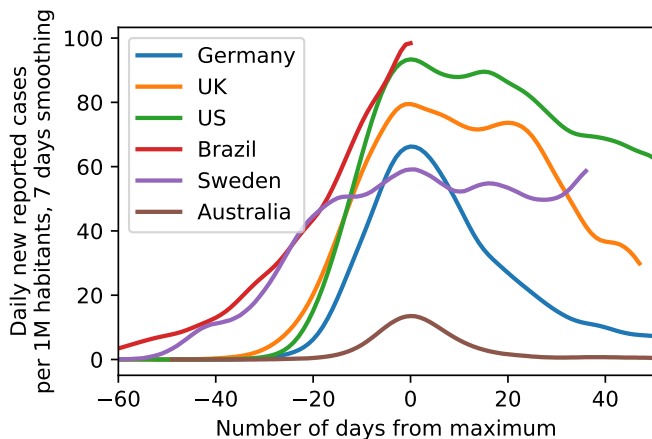


FIG. 7. Comparison of the case numbers per one million inhabitants of exemplary countries as illustration of the range of possible case numbers developments. Note how both the peak height as well as peak width of some countries are considerably larger than for Germany, providing evidence against saturation effects (‘herd immunity’) in Germany (Data until June 3, 2020).

525 does not provide a proof of causality in the strict sense
 526 advocated for example by Pearl [5] or by Ay and Polani [6].
 527 Yet, fulfilling the formal criteria for causality in this strict
 528 sense would need multiple replications of the pandemic
 529 process, each time with different settings of the relevant
 530 variables, such as interventions. Even when treating the
 531 SARS-CoV-2 outbreaks in different countries around the
 532 world, with their different interventions (or lack thereof),
 533 as replications establishing formal causality may remain
 534 an elusive goal due to multiple other variations from
 535 country to country. In sum, the results of our Bayesian
 536 analysis must be seen as a search for the most plausible
 537 causal model of the data, given the data available at the
 538 time of analysis, and as providing credible ranges of the
 539 parameter values relative to this most plausible model.

540 Later, discussions (such as the one presented here) of
 541 the selected models and the inferred parameter ranges
 542 should then investigate and update modeling assumptions,
 543 and reason whether the causal model can be maintained,
 544 or not.

545 When analyzing improved data that reflect the dates of
 546 symptom onset rather than case reports to improve our
 547 modeling, we find that both the preference for a three
 548 change-point model as well as the inferred parameter
 549 ranges do not change drastically, and we maintain our
 550 original interpretation of the pandemic process and the
 551 effectiveness of governmental interventions.

552 Last, alternative models assuming herd immunity as a
 553 reason for the sustained observed drop in infection rates
 554 still do not seem plausible to us in the light of rapidly
 555 surging second waves or sustained high levels of new
 556 infections (such as in Sweden, see Figure 7).

557 IV. MODEL EVOLUTION

558 Modeling efforts at the beginning of an epidemic out-
 559 break are aimed at providing a rough but timely and
 560 robust description of the disease outbreak, making use
 561 of data that is available (and easily accessible) at that
 562 time. Later modeling efforts, in contrast, can make use
 563 of more detailed data and provide deeper insights into
 564 how the outbreak unfolded. While these latter models
 565 are useful for a better understanding after the fact, they
 566 cannot be applied early on due to a lack of data, and often
 567 cannot inform decisions sufficiently fast. However, a com-
 568 parison of early and later models can provide important
 569 insights about the robustness and usefulness of the early
 570 models with respect to the later ones (here usefulness
 571 means that the early models describe the epidemiological
 572 parameters and their uncertainties well enough to inform
 573 decisions). For the case of the COVID-19 outbreak in
 574 Germany, the initially available data were sorted based
 575 on date of reporting, where the reporting occurred after
 576 an unknown delay between symptom onset and report.
 577 Only later, data organized by time of symptom onset, the
 578 so-called epi curve, became available. Even after their
 579 initial release, these data were still updated and refined
 580 (see Fig. 8); also note that data for symptom onsets still
 581 take some time to arrive and be compiled, i.e. the delay
 582 between symptom onset and testing/reporting is still con-
 583 siderable (see Tab. II). In particular, this means that
 584 *reliable* epi curve data for the date of April 21, our analy-
 585 sis cut-off date in [1], were not available on that day but
 586 only considerably later (cf. Tab. II). Now that these data
 587 are available, however, we can compare models based on
 588 data organized by reporting date (modeling the reporting
 589 delay and incubation period) with models based on the
 590 epi curve (modeling the incubation period, only).

591 A. Model updates based on time of symptom onset 592 and comparison to previous results based on time of 593 reporting

594 Ideally, modeling of an epidemic outbreak should rely
 595 on data organized by infection date — yet, such data
 596 are rarely available outside of the analysis of individual,
 597 well-confined infection chains. The next best option are
 598 data organized by date of symptom onset — the epi curve.
 599 Normally, symptom onset precedes the test and report in
 600 time. Thus, the epi curve is only available after a certain
 601 delay, which can be substantial. Furthermore, the time
 602 of symptom onset may remain unknown for a significant
 603 fraction of reported cases. If so, then reconstructing the
 604 epi curve requires data imputation and further modeling
 605 (e.g. nowcasting [7, 8]), which may further delay the avail-
 606 ability of this curve and introduce additional sources of
 607 uncertainty. At the initial stages of an outbreak, one may
 608 therefore decide to analyze data organized by reporting
 609 data, and to model the relevant delays. For a comparison
 610 of analyses, it is important to understand how the curve

of reporting dates and the epi curve are linked. Both curves originate from the curve of initial infections by a convolution (see Fig. 2). The epi curve is the curve of initial infections convolved by the distribution of incubation periods, while the curve based on reporting date is the curve of true infections convolved by the (less well known) distribution of delays between infection data and reporting date. Technically, a report can also happen before symptom onset, albeit this is typically rare¹. Therefore, the curve of reporting dates is not exactly a convolution of the epi curve with an additional delay distribution.

We have reanalyzed the initial stages of the outbreak until April 21 based on the epi curve that has become available (see Figs. 17 and 19), using models with one, two and three change points, based both on SIR and SEIR dynamics (only figures for the three change points models are shown).

These new results do not change our main inference result presented in [1]. Specifically, model comparison still favors the three change point models over their simpler counterparts (see Tab. I), and only the third change point leads to a value of the effective growth rate λ^* that is clearly below zero. Importantly, the growth rate has to be sufficiently below zero to cause a notable decrease in new infections (Fig. 17 H). At the quantitative level, however, we see some evidence for a larger drop introduced by the first change point when using the epi curve data, and smaller drops induced by the second and third change point, especially when using an SEIR model (see Fig. 19). These quantitative changes are driven by the epi curve dropping faster than the curve reflecting reporting date (see Fig. 9 C). Note, however, that we did not yet include in our analysis the uncertainty of the epi curve from the nowcast data imputation, nor did we consider potentially missing data from future reports (cf. Fig. 8 that shows how the epi curve around the maximum was still subject to changes from nowcasts performed mid April to nowcasts performed end May).

TABLE I. Model comparison: Using leave-one-out (LOO) cross-validation, we compare the SIR and SEIR model variants using the epi curve as data (Figs. 17 and 19). Lower LOO-scores represent a better match between model and data (pLOO is the effective number of parameters).

Model	# c-pts.	LOO-score	pLOO
SIR main	0	900 ± 13	6.36
SIR main	1	774 ± 14	12.72
SIR main	2	755 ± 13	12.17
SIR main	3	725 ± 15	19.66
SEIR-like	0	900 ± 14	6.65
SEIR-like	1	749 ± 12	8.05
SEIR-like	2	739 ± 13	10.28
SEIR-like	3	726 ± 14	14.04

¹ In Germany, only for a tiny fraction of cases the reported symptom onset (*Refdatum*) is after testing (*Meldedatum*): 1446 of 130027 cases in the RKI dataset of Jun 11.

In sum, we conclude that the original model based on data organized by reporting date was useful to understand disease dynamics in the absence of the epi curve and robust in the sense that its main results still hold.

B. Differences between results based on RKI versus JHU data sources

At the beginning of the outbreak, data were made available on a daily basis both by Johns Hopkins University (JHU) and the German Robert Koch Institute (RKI). Both sources initially provided only reported cases (in text form), with the JHU resources providing data faster and with a better interface for automated analyses. The RKI resources were updated only a few days later, as information has to be transmitted from regional agencies to the RKI, whereas the JHU data for Germany are gathered from a few reputed online media (Berliner Morgenpost, Tagesspiegel and Zeit Online [9]). However the JHU resources have been partially criticised for lacking quality control (see issues section on the Github page [10]). We therefore compared the JHU data used in [1] to the official RKI count (Fig. 14) and have rerun the analysis using the RKI reported cases (the “Meldedatum”, Fig. 15 and 16). The differences are minor.

V. IMPACT OF TESTING

Our modeling depends on reported case numbers, which in turn depend on testing. Throughout the COVID-19 spread, test availability, test requirements and known case numbers changed continuously over time (Fig. 8). Such an inconsistent and fluctuating data-acquisition obviously introduces additional sources of uncertainty. While we decided to exclude the effects of testing in previous models, concerns about results derived from data that stem from inconsistent testing should be taken seriously. Thus, we analyze possible distortions in more detail.

During the initial outbreak of a disease, it is common that only very preliminary data and statistics on testing is available. This was also the case at the time of writing of our initial manuscript [1]. Since then, several improvements of the available data were implemented. Improvements include details such as testing statistics, but also an estimate of the epi curve (the number of cases based on the date of symptom onset) via imputation and Nowcasting. For the epi curve, complete data on symptom onset is only available for 60% of cases, and the remaining 40% of onsets need to be imputed based on the reporting date[8]. Fortunately, the publicly available RKI database contains both date of onset of symptoms and reporting for individual cases and thus implicitly also the date of testing, which in general is one day earlier than the report. Now, with new data, we come to the conclusion that reported case numbers — although they might derive from variable testing — are still useful to

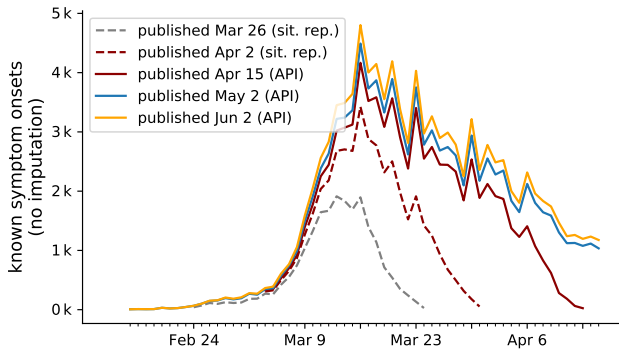


FIG. 8. **The curve of known symptom onset continuously changes over time, as the date of onset of further reported cases is obtained.** Because testing confirms the onset of symptoms in the past with varying delay, the curve not only grows at its tail but over a wide time period with each new publication. **Known** onsets are reproduced from the RKI’s daily situation reports (Mar 26 and Apr 2, read of from respective plots) and the publicly available RKI-database (Apr 15, May 2 and Jun 2). Unknown onsets of symptoms, which account for 40% of total number of cases, are not considered here. Hence the curve on display here is not the full epi curve.

infer the actual disease dynamics. As we will demonstrate below, our major conclusions remain unchanged.

In particular, evidence for the key characteristics of the first wave — strong exponential growth in new cases, change in transmission dynamics over a limited time period and slow exponential decline — can be derived from the available data, even if changes in testing are considered.

To investigate the impact of testing, we first focus on two central quantities: i) the number of tests that are performed, say, on a given day or in a given week and ii) the fraction of the performed tests that are positive — a positive tests translates to a confirmed case.

Let us consider two simple limiting cases, in which only one of these quantities changes and the other one remains constant: If a constant number of tests is performed day-after-day and we observe a growing fraction of positive test results, this corresponds to an increase of the underlying case numbers. Conversely, if the number of tests is increased and we find a constant fraction of positive tests, this also implies an increase of the underlying case numbers². Fig. 9 A, B shows that in Germany in early March both, the number of tests as well as the fraction of positives increased simultaneously. This simultaneous increase indicates a significant growth in new case numbers.

² The second case only holds with additional assumptions: i) the fraction of positive tests is larger than the prevalence and ii) tests are not performed randomly, both of which were met in Germany.

727

A. Strong growth of new cases until week 12

728

By focusing on testing before week 12 in Fig. 9 A and B, we can deduce a strong growth in daily new cases, as both the fraction of positives as well as the number of performed tests rise (matching the combined two scenarios above).

729

For the time before week 12, the number of tests changed week-to-week and a direct link between the test fraction and the reported cases does not hold. However, we can assume a constant level of testing within one week (Fig. 8 in [11]). At the same time, we see a continuous increase in the fraction of positives within the week (Fig. 9 B). Especially going from week 11 to week 12, where we have both, an increase in testing (from week-to-week) and an overall increase in the fraction of positives (from day-to-day), this implies a strong growth of new infections.

733

For weeks 12 onward, the number of performed tests stays roughly constant. Thus, the fraction of positive tests directly links to the number of reported cases, and both indicate a decline in the underlying (true) case numbers that starts in week 14. This conclusion is further supported by the high level of testing that starts in week 12: Testing at a constant *and* high level makes the fraction of positives a reliable indicator of case numbers.

732

Hypothetical Scenario: If we were to reject the above simple explanation that growing case numbers reflect growing numbers of infections, there is one alternative scenario to explain the observed trend. As this scenario has frequently occurred in the public debate on the spread of COVID-19 in Germany, we discuss it briefly.

735

The underlying assumption in this scenario is that the few tests that were performed during the initial outbreak until week 11 missed most of the actual cases, i.e. a large pool of infected persons would have existed unobserved. Then, at the same time at which the amount of tests was increased from week 11 to 12, coincidentally the effectiveness of the testing could have increased, so that the unobserved pool (of constant size!) is identified and, thus, apparent case numbers rise. Given the rigorous criteria (based on symptoms and risk of exposition) that were required from patients in order to qualify for one of the early tests, we deem this scenario of an unobserved and constant pool to be quite unlikely.

736

B. The reporting delay relates reported cases to disease dynamics

737

We here focus on the disease dynamics that shape the peak of the epi curve, corresponding to the maximum new daily infections (see again Fig. 9, C, red). We notice that the increase of the fraction of positives tests (gray) continues longer and more smoothly than the increase in the epi curve (red). Thus, in the following, we discuss that testing from week 12 on reliably describes the epi curve in weeks 11–13. In general, we find as a rule of

740

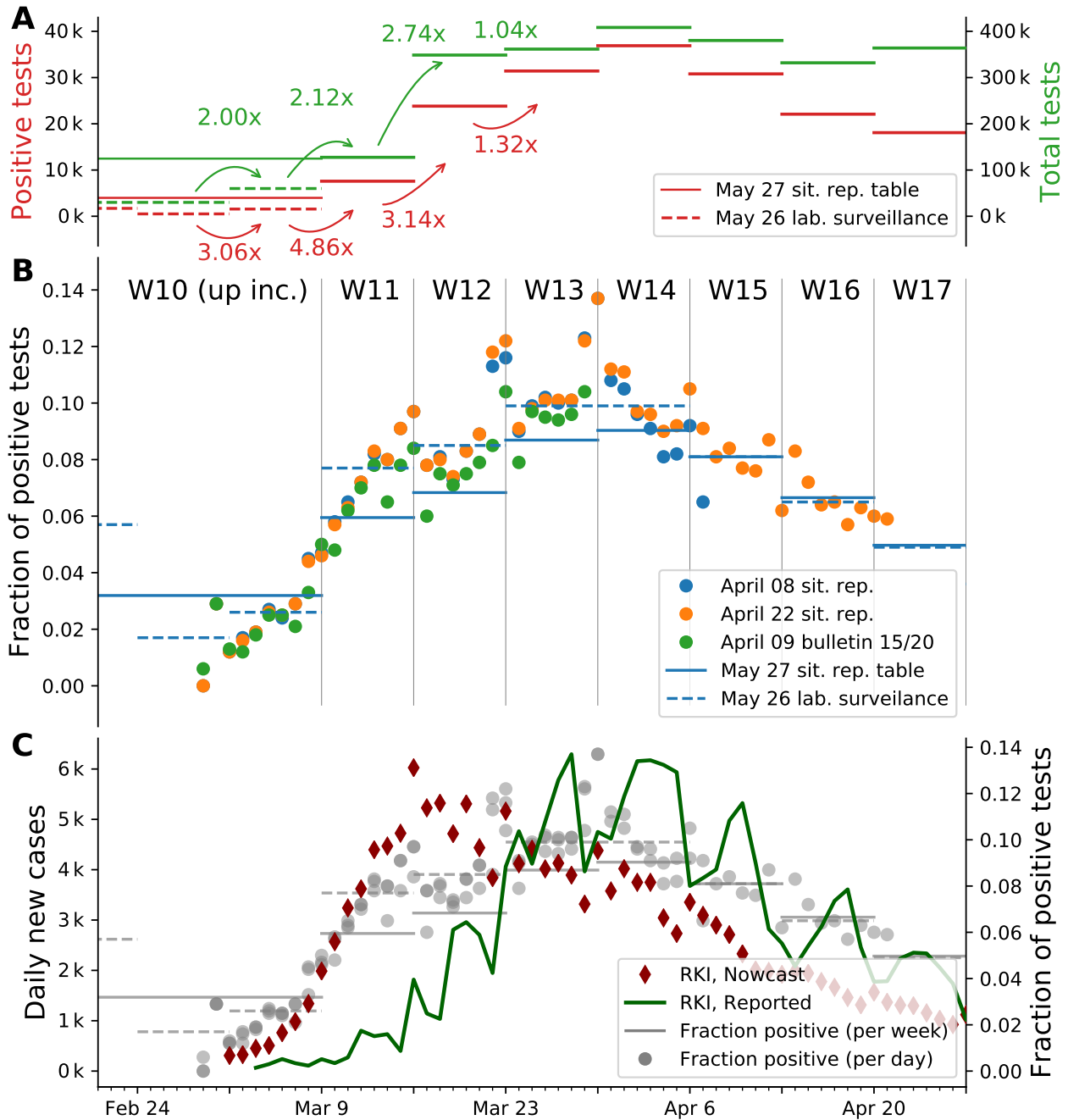


FIG. 9. **Weeks 10 to 12 show strong growth in in the number of new cases, which was not limited by the early testing capacity.** **A:** Comparison of number of positive test results with the number of tests performed for each week. Reproduced from Table 5 in [11] and extrapolated from [12]. Note: Numbers for week 10 and earlier are represented by a single data point in the first source and individually in the latter. The week-over-week increase uses available weekly data. **B:** Mid-term changes in the fraction of positive tests is more obvious in the daily data (points) than in the weekly (bars), especially in early March. Daily values are taken from situation reports [11, 13, 14] (full dataset) and the epi bulletin [12, 15] (ARS dataset). Weekly values, represented as horizontal lines, are taken from a situation report table and a weekly lab surveillance report (ARS dataset). Note: the latter represents a subset of all tests. Compared to the situation report, the ARS dataset lists weeks 8 to 10 individually. **C:** Overlay of Panel B with the number of cases reported per day by the RKI and the estimated epi curve (imputation and Nowcasting, as described in [8]). The fraction of positive tests correlates with the number of reported cases from week 13 onward, as the total number of tests reaches a constant level.

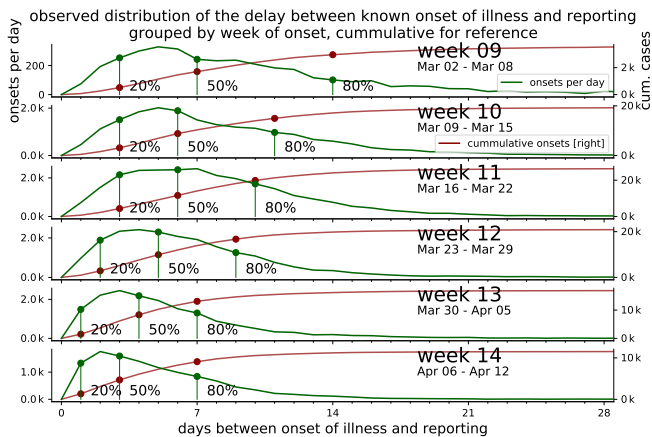


FIG. 10. The onsets of symptoms are confirmed by testing at a later and varying point in time, which accounts for most of the delay until all or the main fraction of known onset of symptoms (*IstErkrankungsbeginn* in RKI-database) are reported. From the RKI data, the number of cases per delay between onset of illness and reporting (i.e. *RefDatum* and *Meldedatum*) for cases with known onset of symptoms (*IstErkrankungsbeginn*) are counted for each week. The fraction of reported cases out of the total onsets up to a delay are highlighted for 20%, 50% and 80%. The cumulative number of cases reported up to each delay is displayed for reference.

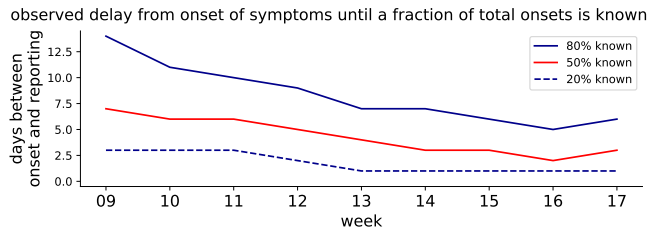


FIG. 11. The reporting delay decreases from week 9 to week 14. Grouped by week, the delay between onset of symptoms and the reporting of 20%, 50%, 80% fractions of all known onsets is shown (cf. dots in Fig. 10).

thumb that the majority of positive tests of week i have onsets in week $i - 1$.

The key is the connection between the date of symptoms onset (when symptoms first show), the testing (when the symptom onset is confirmed or an asymptomatic case is uncovered), and the reporting date (when a positive test-result is registered). Any reported case must inherently be preceded by a test and according to the RKI, positive test results are reported within 24 hours to the responsible health department. Thus, the date of testing is taken as the day before reporting in the rest of the analysis. The remaining task is to reveal the connection between symptom onset and reporting date, i.e. the reporting delay for each individual case.

In Fig. 10, we detail the reporting delay by plotting distributions of how many days after the symptom onset a case is reported. For example, if each and every infected

person would receive a test result (become a reported case) exactly three days after they showed symptoms, then the plotted distributions would have only one entry: a delta-peak at three days. However, we see that most reports arrive 1–7 days after symptom onset, where the details of the (lognormal) distribution depend on the week of onset of symptoms.

Heavy tails in the distributions correspond to long reporting delays. Until and including week 12, the distributions have heavy tails. After week 12, the distributions have lighter tails. This provides some intuition of the distributions and the meaning of the heavy tails: most of the symptom onsets are reported within the first week but some will be reported much later, so that the shape of the distribution still keeps changing. If the test level is low, more cases will be reported later and the tails of the distribution are heavier. This latter effect is what we see for the onsets during the first weeks until 11; due to limited testing capacities, many cases were only reported weeks later — once more testing was available.

The distributions of the reporting delay give information about how timely the reporting is, on average (Fig. 11). Focusing on week 11, 20% of all the onsets of symptoms that were found to be in this week were reported very quickly, within 2.5 days (blue dashed line). Within 5 days, half of all onsets have been reported (red solid line) and within 9 days, the fraction of onsets from this week that have been reported rises to 80% (blue solid line). As a practical example, let us look at the onsets that occurred on Wednesday of week 11: Half of all onsets get reported very quickly, until Sunday, and the remaining half is only reported over the following weeks.

This example also hints at a dependence of the reporting delay on the weekday. Clearly, less tests are performed during weekends. Hence, if a symptom onset occurs on Monday, it is more likely to be tested and reported within the same week than if it occurs on Friday. For later days of the week, the fraction of tests (and cases) that is performed (and reported) not in the same week but only in the next week rises systematically.

The shape of the distributions (Fig. 10) and the weekday-dependence motivate the rule of thumb mentioned earlier: 80% of all the symptom onsets that occur in a given week are reported by the end of the following week. However, due to the weekday-dependence, only around half of all onsets are found within the same week — much less during weeks 9–11, when testing was at capacity limits. In conclusion, high test levels in week i give confidence in the epi curve of week $i - 1$.

C. Decomposing the epi curve into weeks of testing

Having established the delay between symptom onset and reporting, we can decompose the epi curve and identify parts of the curve that stem from certain weeks of testing. We do so by reconsidering the reporting delay. We may ask: *Given the test results of a chosen week,*

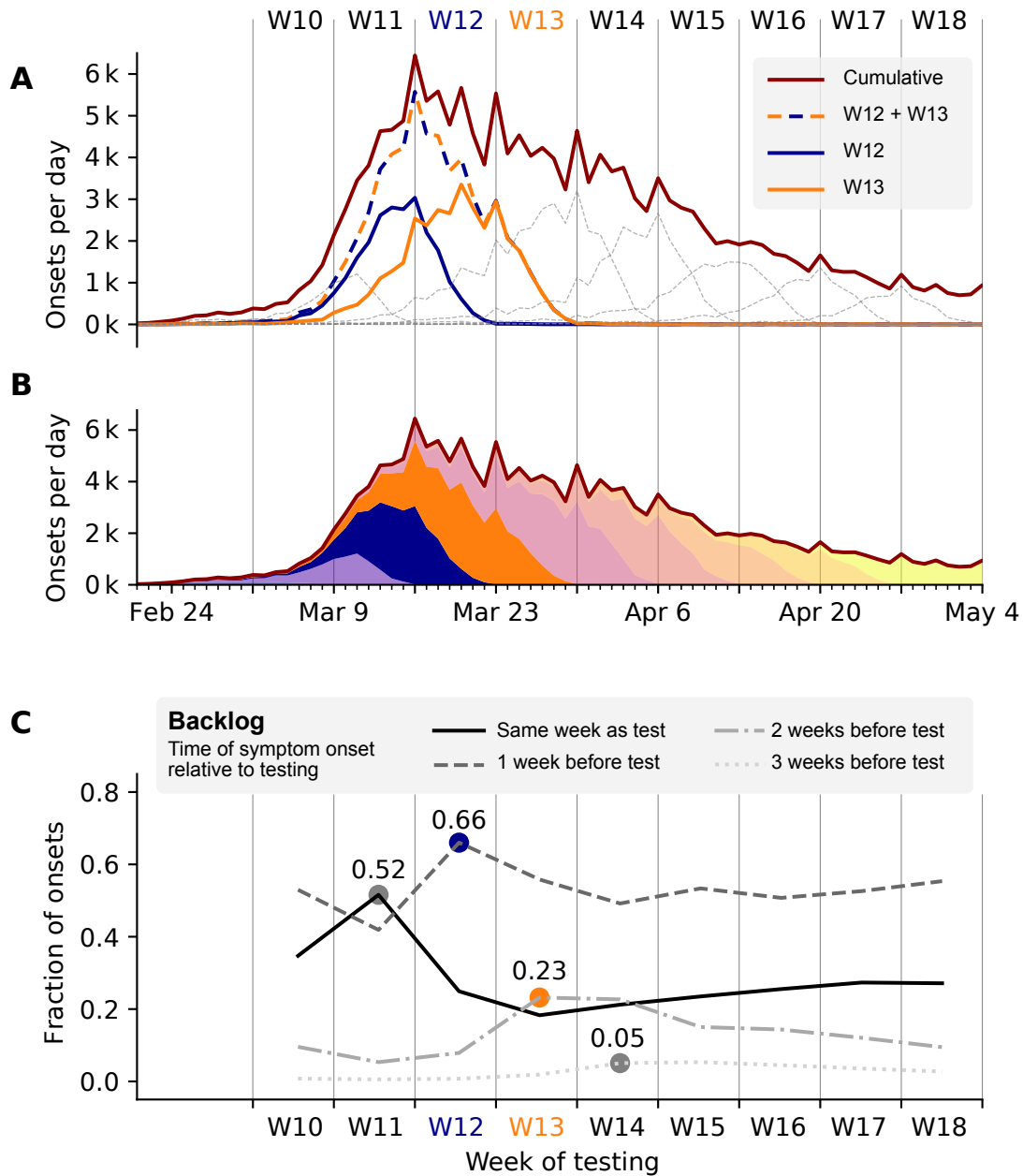


FIG. 12. Testing in one week confirms onsets of symptoms that occur up to 4 weeks earlier. The extend of this effect is analyzed based on the RKI database through decomposition by allocation of onsets of symptoms to weeks of testing. It is assumed that the delay between the time of testing and *Meldedatum* is 1 day. Tue-Mon *Meldedatum* is taken as a proxy for Mon-Sun testing. **A** Onsets of symptoms per day curves allocated to weeks of testing, weeks 12 and 13 are highlighted. Most known onsets around the peak of the epi curve in week 11 are confirmed by the testing in weeks 12 and 13. **B** stacked decomposition of the epi curve into weeks of testing. **C** To reveal crucial information about week-to-week change in the number of total onsets based on one week of testing, the shape of the distributions of onsets of symptoms confirmed by that week of testing is characterized. The fraction of onsets in the same week and each preceding week out of the total onsets confirmed by the week of testing is calculated. This indicates, the portion of a week's positive tests confirming onsets in the same week or in preceding weeks (max. 3 weeks earlier). The evolution of these 4 values is plotted by the week of testing. The peak of the epi curve can be tracked through testing results of weeks 11 to 14 as a maximum in the same-week/n-weeks earlier fraction of onsets confirmed in those respective weeks: 52% of all cases confirmed through testing in week 11 had onset of symptoms in the same week. Even more notable: 66% of positive tests in week 12 are linked to onsets 1 week earlier: in week 11. For comparison, see Fig. ??

853 *how are the dates of symptom onset that we found in the*
 854 *chosen week distributed over the previous weeks?*

855 In Fig. 12 A, B we collect all the symptom onsets
 856 that were found by testing in week 12 (blue), in week 13
 857 (orange) and in both weeks combined (dashed). As we
 858 see, the peak of the full epi curve (red) on March 16 is
 859 dominantly composed of cases that were tested in week
 860 12 and 13, weeks that already featured the high level of
 861 testing. This decomposition — which part of the curve
 862 stems from which tests — further confirms what we saw
 863 earlier: high testing in a week gives confidence in the epi
 864 curve of the previous week.

865 With the decomposition of the epi curve at hand, we
 866 may pick one particular week of testing and compare the
 867 number of onsets in different weeks that were confirmed
 868 in the testing-week we picked. In other words, we are
 869 interested in the *distribution of onsets per week seen by*
 870 *the testing in one single week.*

871 As viewed from one single week of testing, we distin-
 872 guish four categories according to the delay between onset
 873 and testing (Fig. 12 C): onsets in the same week as the
 874 test (solid), onsets one week earlier than the test (dashed),
 875 onsets two weeks earlier (dash-dotted), and onsets three
 876 weeks earlier (dotted). By comparing the fraction of cases
 877 in these categories week-over-week, we can reveal the *back-*
 878 *log of testing.* The backlog of testing corresponds to the
 879 last three categories; it describes how many cases were not
 880 tested within the same week (different dashing). Looking
 881 at the backlog week-over-week helps us to identify weeks
 882 during which the limit of testing capacity might have
 883 been reached or the testing policy might have changed.

884 When considering the respective maxima of the backlog-
 885 categories (colored dots in Fig. 12), we find that backlog
 886 was build up especially during week 11. In week 11, most
 887 onsets stem from the same week (52%, maximum of the
 888 solid line). At the same time, in week 11 there was very
 889 little backlog; only few cases from previous weeks were
 890 found (minima of the dashed lines). In week 12, we find
 891 that most cases stem from the previous week — namely
 892 week 11 (66%, maximum of the dashed line). This trend
 893 continues in weeks 13 and 14, which exhibit comparably
 894 high fractions of onset 2 weeks and 3 weeks earlier,
 895 respectively, each pointing to week 11 (maxima marked
 896 by dots). Together, this (self-consistently) supports the
 897 strong growth of new onsets especially during week 11; a
 898 strong rise of cases before week 11 is less likely because it
 899 did not manifested in the backlog.

900 D. Available data on testing

901 The epi bulletin [16] outlines the different networks that
 902 the RKI uses to source information on testing: *Voxco*,
 903 *RespVir*, the antibiotics-resistance-surveillance (ARS) [12]
 904 and lab-association queries. These sources are compiled
 905 into weekly data-sets with total number of tests and posi-
 906 tive tests, which are published in the daily situation report
 907 once a week.

908 Data from the ARS contains daily number on testing and
 909 a separate weekly report is published on the RKI website.
 910 The ARS dataset covers 25-30% of the total number of
 911 tests reported by the RKI, as only 62 of 180+ labs par-
 912 ticipate. The ARS data-set shows a mean delay between
 913 sampling and testing between 1 and 1.2 days except for
 914 weeks 12 to 15, where the delay is 1.5 days, peaking in
 915 week 13 at 1.8 days.

916 An overview of all publicly available data on testing for
 917 march 2020 is presented in Fig 9. The following observa-
 918 tions along with additional comments are based on this
 919 presentation:

- 920 • From week 8 to week 12 the number of tests rises
 921 week to week by a factor greater than 2. 120k is a
 922 combined number for weeks up to 10. Individual
 923 numbers of tests for those weeks has to be estimated
 924 with help from the ARS-subset (Fig. 9 B *may26*
 925 *lab. Surveillance*). Assuming ARS is representative
 926 the number of test performed in week 10 should
 927 be around 60k, 30k in week 9 and 30k in all weeks
 928 up to and including 8, extending the exponential
 929 pattern.
- 930 • The number of tests remains on a high level from
 931 week 12 on. In the range of 340-430k.
- 932 • The number of positive tests rises faster than the
 933 total number of tests until week 14.
- 934 • The fraction of positive tests per week peaks around
 935 10%, relatively low compared with neighbouring
 936 countries.
- 937 • The fraction of positive tests per day varies with
 938 time from 2% around March 1 to around 10% in
 939 weeks 13 and 14, peaking at 14% at the end of
 940 March. Afterwards declining to less than 2% in
 941 week 20 (not shown in figure). The day-to-day rise
 942 in week 10 and 11 is more pronounced than the
 943 weekly average would suggest.
- 944 • The increase in the fraction of positive tests does
 945 not correlate to the rise in number of reported cases
 946 until week 13, but correlates with the decline in
 947 reported cases from week 13 on, which is expected
 948 as the total number of tests fluctuates around 380k
 949 tests per week on a high level.
- 950 • The ARS data shows a steady day to day increase in
 951 positive fraction of test in weeks 10 and 11. Week-
 952 ends show a higher fraction, while the total number
 953 of tests is lower (daily total number not shown in
 954 the figure). Deviating from the rise in the positive
 955 fraction, weeks up to 8 have a 3 times higher fraction
 956 of positive results than week 9.
- 957 • The maximum test-capacity per week as reported by
 958 the labs increased to 1M in week 19, showing strong
 959 growth until week 14. A week to week doubling in
 960 test capacity continues for two more weeks compared
 961 to growth in number of tests performed (not shown).

962 For the total data-set, the fraction of positive tests varies
 963 from 1.5 to 7.2% for different states. Not a single day of
 964 testing for individual states exceeded 20% positive results.

965 VI. BEHAVIORAL CHANGES AND 966 INTERPRETATION OF RESULTS.

967 Work in progress.

968 VII. SUMMARY & CONCLUSIONS

969 In these technical notes, we have comprehensively ad-
 970 dressed questions and comments regarding our recent
 971 publication [1]. First, we compared direct, model-free es-
 972 timates of the reproduction number to the ones obtained
 973 from dynamical modeling. To this end, we established
 974 synthetic ground-truth data based on an SIR model and
 975 subsequently inferred the reproduction number based on
 976 various complementary approaches that are in practical
 977 use. We revealed how sudden changes in the spreading
 978 rate — as expected from the broad and swift implementa-
 979 tion of non-pharmaceutical interventions and concurrent
 980 changes in behavior — can lead to counter-intuitive tran-
 981 sient drops in new reported cases. Most importantly, we
 982 found that modeling of spreading dynamics can correctly
 983 capture effects of sudden changes in the spreading rate.

984 Second, we provided extensive background on our mod-
 985 eling rationale, which combines differential-equation based
 986 modeling of dynamics with Bayesian parameter inference
 987 and formal model comparison. Within the Bayesian frame-
 988 work, we argued that based on prior knowledge, the most
 989 plausible models explaining the data can be systematically
 990 identified and also updated as new information becomes
 991 available. We also discussed why we do not think that
 992 strong effects of herd immunity are plausible given our
 993 present knowledge.

994 Third, we analyzed additional data on the SARS-CoV-
 995 2 spread in Germany, which has become available since
 996 the completion of the analysis presented in [1]. Most

997 importantly, we included data sets from the German
 998 Robert Koch Institute based on the reporting date as
 999 well as based on the onset of symptoms (epi curve). We
 1000 analyzed the data in the framework of SIR and SEIR
 1001 models, and we also tested a broad range of varying prior
 1002 assumptions. We found our central results to be robust
 1003 across these varying modeling assumptions and data sets,
 1004 and to support the conclusions drawn in [1]. In turn, this
 1005 lead us to conclude that under the conditions comparable
 1006 to those in Germany, models based on reporting date are
 1007 a viable alternative for analyzing the early stages of a
 1008 disease outbreak, before the epi curve becomes available
 1009 — as long as the reporting delay is properly modeled.

1010 Finally, we addressed the issue of changes in the testing
 1011 capacities and procedures over the course of our analysis.
 1012 Most importantly, we found that, while data from the
 1013 initial onset of the pandemic is presumably affected by
 1014 a rise in test capacities, the crucial part of our analysis
 1015 is based on a regime of comparably stable testing. In
 1016 particular, we concluded that the inference of the second
 1017 and third change point is widely unaffected by testing.

1018 Overall, the analysis here evaluated the robustness of
 1019 our previously reported results with respect to statistical
 1020 and dynamical modeling assumptions as well as comple-
 1021 mentary data sources and provided additional support for
 1022 the central conclusions of our publication [1]:

- 1023 1. combining epidemiological modelling with Bayesian
 1024 inference enables a robust assessment of the spread-
 1025 ing of infectious diseases in a timely manner;
- 1026 2. the spreading dynamics can only be inferred with a
 1027 considerable delay (due to incubation periods and
 1028 testing/reporting delays);
- 1029 3. applied to the COVID-19 outbreak in Germany,
 1030 it appears most plausible that all interventions to-
 1031 gether with the concurrent change in behavior re-
 1032 duced the effective growth rate λ^* , and that λ^*
 1033 dropped substantially below zero close to the time
 1034 of the third intervention.

-
- 1035 [1] J. Dehning, J. Zierenberg, F. P. Spitzner, M. Wibral, J. P.
 1036 Neto, M. Wilczek, and V. Priesemann. Inferring change
 1037 points in the spread of covid-19 reveals the effectiveness
 1038 of interventions. *Science*, 2020.
 1039 [2] Theodore Edward Harris. *The Theory of Branching Pro-*
 1040 *cesses*. Grundlehren der mathematischen Wissenschaften.
 1041 Springer-Verlag, Berlin Heidelberg, 1963.
 1042 [3] Erläuterung der Schätzung der zeitlich variierenden
 1043 Reproduktionszahl R/7-Tages-R, [https://www.rki.de/DE/Content/InfAZ/N/Neuartiges_Coronavirus/](https://www.rki.de/DE/Content/InfAZ/N/Neuartiges_Coronavirus/Projekte_RKI/R-Wert-Erlaeuterung.html)
 1044 [Projekte_RKI/R-Wert-Erlaeuterung.html](https://www.rki.de/DE/Content/InfAZ/N/Neuartiges_Coronavirus/Projekte_RKI/R-Wert-Erlaeuterung.html).
 1045 [4] Edwin T Jaynes. *Probability theory: The logic of science*.
 1046 Cambridge university press, 2003.
 1047 [5] Judea Pearl. *Causality: Models, Reasoning and Inference*.
 1048

- Cambridge University Press, Cambridge, U.K. ; New York,
 2nd edition edition, September 2009.
 [6] Nihat Ay and Daniel Polani. Information flows in causal
 networks. *Advances in Complex Systems*, 11(01):17–41,
 February 2008.
 [7] Michael Höhle and Matthias an der Heiden. Bayesian now-
 casting during the STEC O104:H4 outbreak in Germany,
 2011. *Biometrics*, 70(4):993–1002, 2014.
 [8] M. an der Heiden and O. Hamouda. Schätzung der
 aktuellen Entwicklung der SARS-CoV-2-Epidemie in
 Deutschland – Nowcasting. *Epidemiologisches Bulletin*,
 2020(17):10–15, 2020.
 [9] Tagesschau.de. Exklusiv: Woher die Johns-Hopkins-
 Zahlen zu Corona stammen, <https://www.tagesschau.de>.

available since	source	machine readable	manual extraction needed	reported cases	known symptom onsets	imputed symptom onsets	nowcasting	notes
Jan 22 [17]	JHU dashboard (ArcGIS)		x	x				
Feb 2 [18]	JHU dashboard (GitHub)	x		x				first commit with case numbers on Feb 4
Mar 4 [19]	RKI situation report (pdf)		x	x	x			
Mar 20 [20]	RKI dashboard (ArcGIS)		x	x				known symptom onsets added ~2nd half of April
Apr 6 [21]	RKI dashboard (API, csv)	x		x	x			
Apr 9 [22]	RKI Epi Bulletin (pdf)		x	x	x	x	x	nowcasting introduced in bulletin 17/20v1, includes R_t estimate, note the transient $R < 0$
Apr 15	RKI situation report (pdf)		x	x	x	x	x	nowcasting initially only in German
May 11 [23]	RKI resources on nowcasting (xlsx)	x		x	x	x	x	includes R_t estimate

TABLE II. **Data sources differ in availability, the detail they provide, and accessibility.** For our previous study [1], modelling needed to be fast; we used the JHU data from GitHub because it was available early, it is easy to access (machine readable) and it is the unofficial go-to resource on case numbers. Note that some sources (red cross) need manual extraction of the data from a plot — a process that, even when assisted [24], introduces uncertainties. Also note that only some of the listed sources are accessible in a past, as-was state (for instance, the dashboards only display the most recent data, in real-time).

1063	de/inland/johns-hopkins-uni-corona-zahlen-101.html .	1092	[20]	First appearance of the RKI dashboard, https://twitter.com/rki_de/status/1241057746679746560/ .
1064		1093		
1065	[10] CSSEGISandData. COVID-19, June 2020. original-date: 2020-02-04T22:03:53Z.	1094	[21]	Creation date of the public rki api/csv, https://www.arcgis.com/home/item.html?id=f10774f1c63e40168479a1feb6c7ca74 .
1066		1095		
1067	[11] Täglicher Lagebericht des RKI zur Coronavirus-Krankheit-2019 2020-05-27, 2020.	1096	[22]	First appearance of covid-19 numbers in the rki epi bulletin, https://www.rki.de/DE/Content/Infekt/EpidBull/epid_bull_form.html .
1068		1097		
1069	[12] SARS-CoV2-Surveillance - Wochenbericht vom 26.05.2020, 2020.	1098	[23]	First available nowcasting data table, http://web.archive.org/web/*/https://www.rki.de/DE/Content/InfAZ/N/Neuartiges_Coronavirus/Projekte_RKI/Nowcasting.html .
1070		1099		
1071	[13] Täglicher Lagebericht des RKI zur Coronavirus-Krankheit-2019 2020-04-22, 2020.	1100	[24]	Ankit Rohatgi. Webplotdigitizer.
1072		1101		
1073	[14] Täglicher Lagebericht des RKI zur Coronavirus-Krankheit-2019 2020-05-22, 2020.	1102	[25]	RKI - Coronavirus SARS-CoV-2 - Nowcasting und R-Schätzung: Schätzung der aktuellen Entwicklung der SARS-CoV-2-Epidemie in Deutschland, https://www.rki.de/DE/Content/InfAZ/N/Neuartiges_Coronavirus/Projekte_RKI/Nowcasting.html , downloaded May 22.
1074		1103		
1075	[15] A. Hoffmann, I. Noll, N. Willrich, A. Reuss, M. Feig, M.J. Schneider, T. Eckmanns, O. Hamouda, and M. Abu Sin. Laborbasierte Surveillance SARS-CoV-2. <i>Epidemiologisches Bulletin</i> , 2020(15):5–9, 2020.	1104		
1076		1105		
1077	[16] J. Seifried and O. Hamouda. Erfassung der SARS-CoV-2 Testzahlen in Deutschland. <i>Epidemiologisches Bulletin</i> , 2020(15):3–4, 2020.	1106		
1078		1107		
1079	[17] First appearance of the jhu dashboard, https://systems.jhu.edu/research/public-health/2019-ncov-map-faqs/ .	1108	[26]	RKI COVID19, https://npgeo-corona-npgeo-de.hub.arcgis.com/datasets/dd4580c810204019a7b8eb3e0b329dd6_0 , downloaded June 22.
1080		1109		
1081	[18] First commit in jhu github repository, https://github.com/CSSEGISandData/COVID-19/graphs/commit-activity .	1110		
1082		1111		
1083	[19] First appearance of the rki situation report, https://www.rki.de/DE/Content/InfAZ/N/Neuartiges_Coronavirus/Situationsberichte/Archiv_M%C3%A4rz.html .	1112		
1084		1113		
1085		1114		
1086				
1087				
1088		1115		
1089		1116		
1090				
1091				

VIII. SUPPLEMENTARY INFORMATION: FIGURES

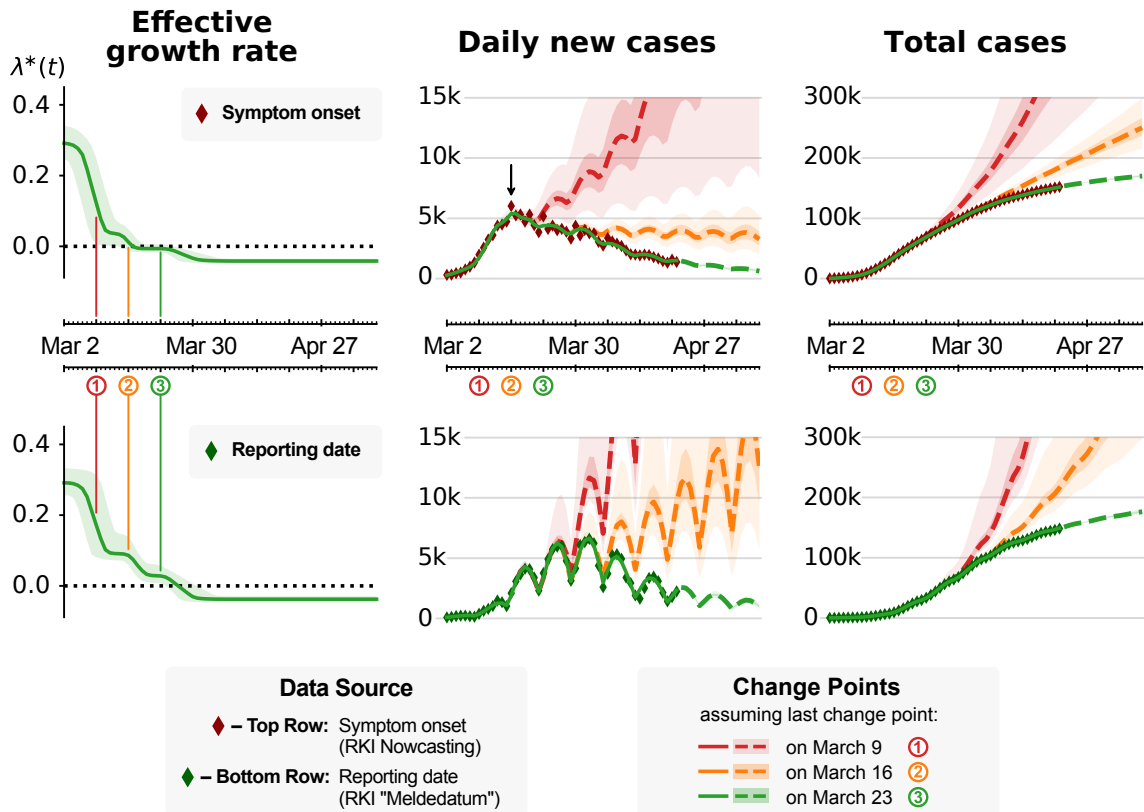


FIG. 13. Model-based inference is consistent when based on symptom onset (top) or reporting date (bottom). We repeated our SIR-model based inference (Fig. 3 in [1]) that used JHU data [10], now using the date of symptom onset (red diamonds, top) [25] and the reporting date (green diamonds, bottom) of daily new cases as reported by the RKI [26]. **Note:** We currently do not incorporate the uncertainties that are introduced by nowcasting (red diamonds, top), compared to using the reported cases. This leads to *over-confident* parameter estimates, including the effective spreading rate $\lambda^*(t)$; the shown uncertainties are underestimated. **Left:** Effective growth rate $\lambda^*(t)$ inferred by the model. Dates of the three main public interventions are indicated by colored circles and vertical lines. The values of $\lambda^*(t)$ before and after *all* change points is consistent across both data sources. Note that, when the symptom onset is used, $\lambda^*(t)$ drops to zero already after the second change point. Still, only after the third change point $\lambda^*(t)$ becomes sufficiently negative to cause *decreasing* daily new case numbers. **Center:** Daily new case numbers. Dashed lines show inferred case numbers assuming that the last two (red) or the last one (orange) change points were excluded. The weekday-dependence in daily new reported cases is already accounted for when using symptom onsets (top). **Center, Top:** Although $\lambda^*(t)$ already dropped to (slightly-below) zero as of the second change point, daily new cases do not decrease if the third change point is excluded (orange). Note the arrow: Due to the transient decrease in new cases after change points (cf. Fig. 4) as well as the delay between symptom onset and reporting (cf. Fig. 4), the peak that corresponds to maximum daily new infections is located already around March 16 (for symptom onsets); yet note again that this does *not* mean that new cases would have declined rapidly already after the second change point (see the orange curve). **Right:** Total, cumulative case numbers.

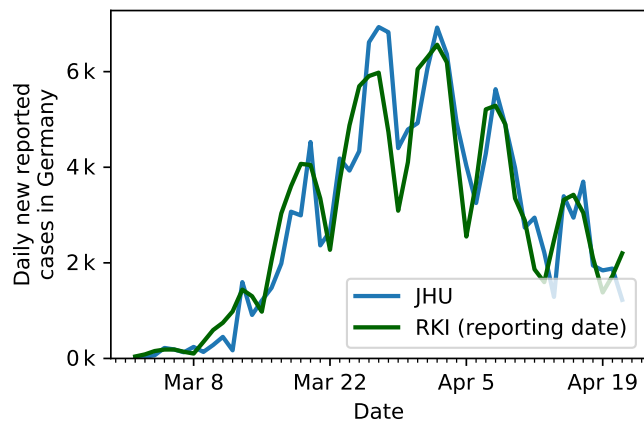


FIG. 14. Comparison of the German case numbers as published by the Johns Hopkins University (JHU) used in our previous publication [1], to the case number of the Robert Koch Institute (RKI).

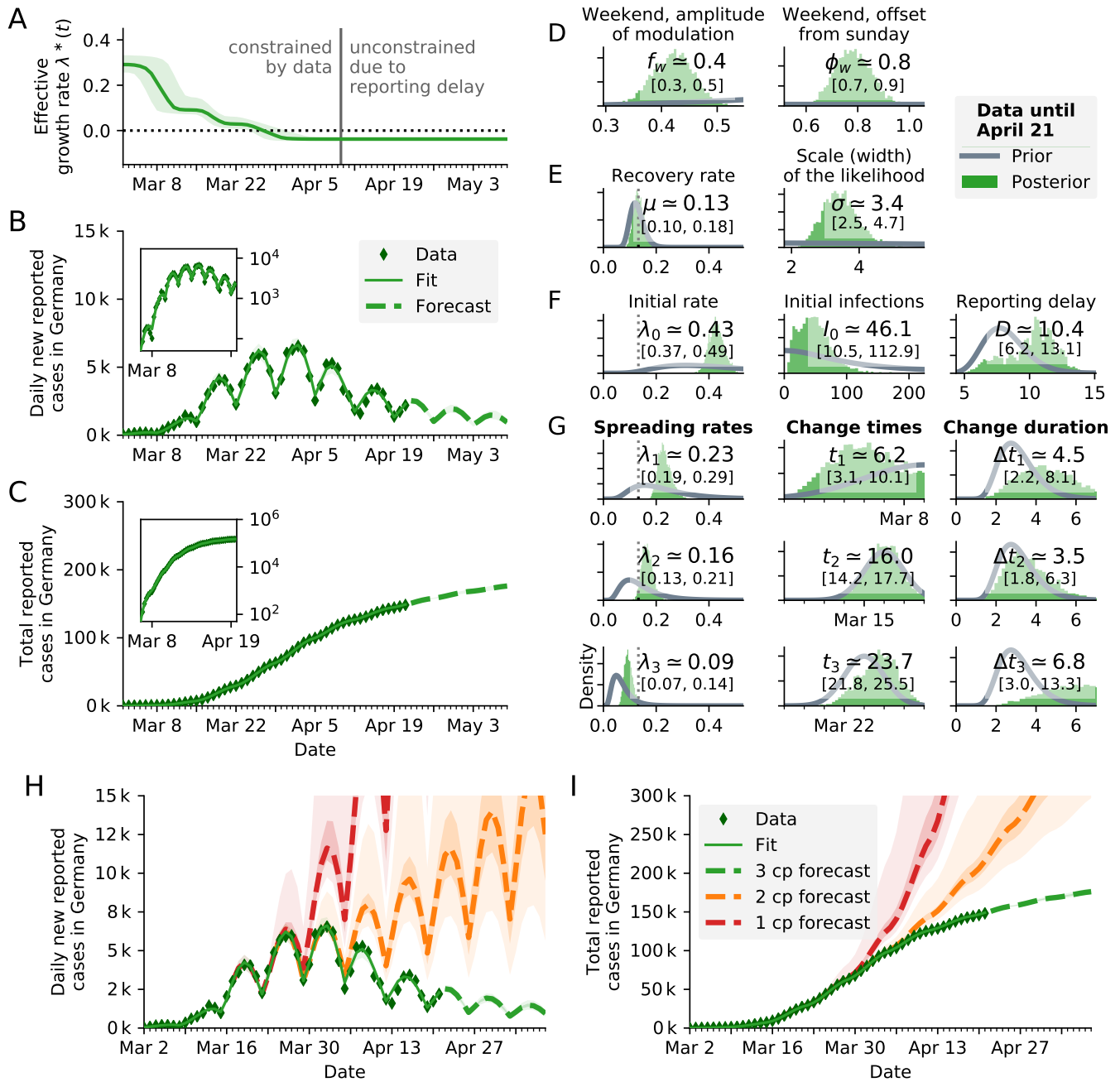


FIG. 15. **SIR model** (see Fig. 3 of [1]) using the **reporting date (Meldedatum)** of the **RKI data** for inference. **A**: Time-dependent model estimate of the effective spreading rate $\lambda^*(t)$. **B**: Comparison of daily new reported cases and the model (green solid line for median fit with 95% credible intervals, dashed line for median forecast with 95% CI); **inset** same data in log-lin scale. **C**: Comparison of total reported cases and the model (same representation as in B). **D–G**: Priors (gray lines) and posteriors (green histograms) of all model parameters; inset values indicate the median and 95% credible intervals of the posteriors. **H–I**: The fitted model with two alternative forecasts. We consider in addition one scenario where only one intervention happened (red) and one where two interventions happened (orange). Includes 50% and 95% CI.

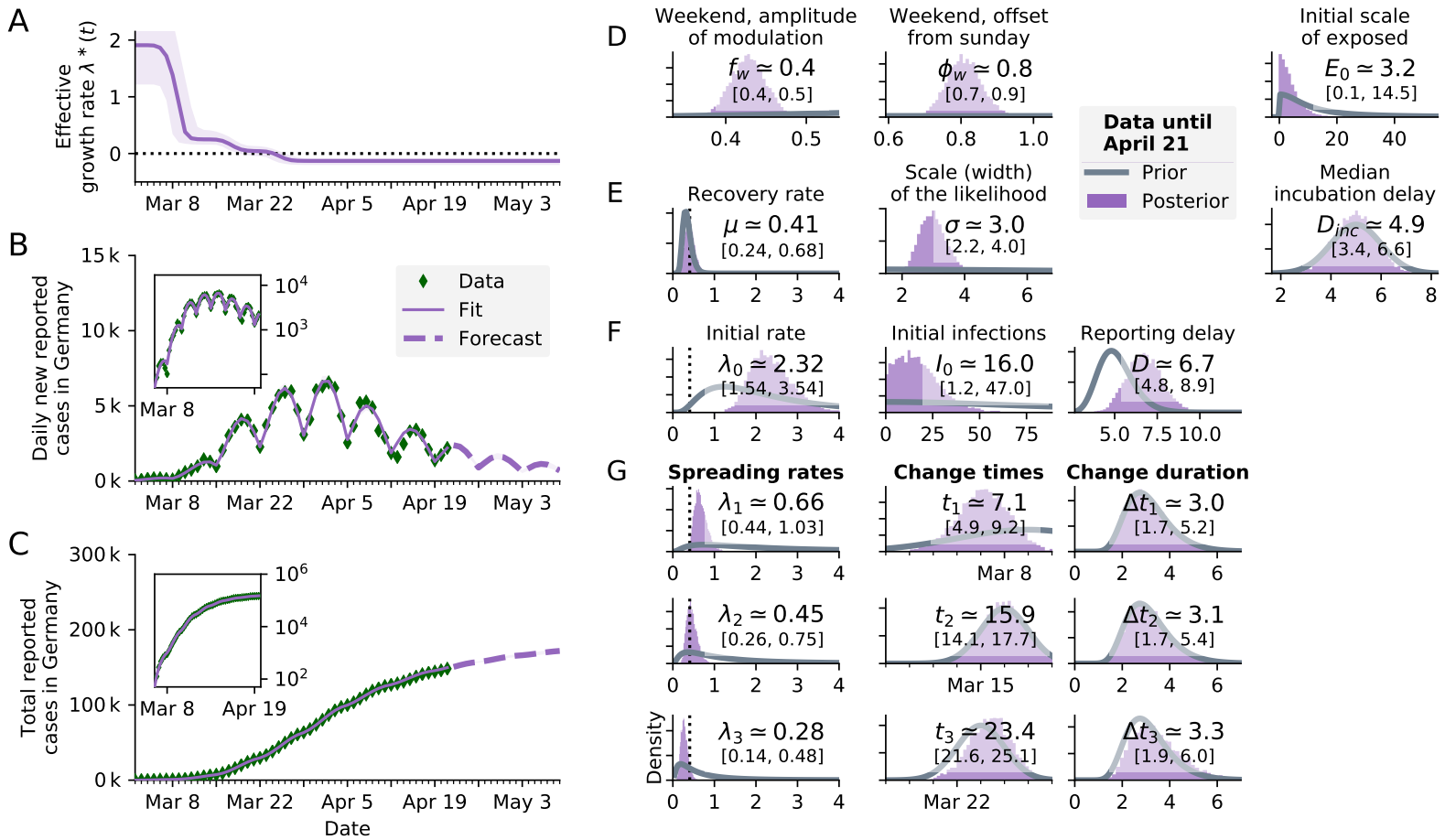


FIG. 16. **SEIR-like model** (see Fig. S3 in Supplementary Information of [1]) using the **reporting date (Meldedatum) of the RKI data** for inference. **A**: Time-dependent model estimate of the effective spreading rate $\lambda^*(t)$. **Note**: Due to different model dynamics, $\lambda^*(t)$ can only be compared *qualitatively* between SEIR and SIR models. The numeric values of the rates (μ , λ etc.) differ between models because they reflect the duration a person remains in a given compartment. **B**: Comparison of daily new reported cases and the model (purple solid line for median fit with 95% credible intervals, dashed line for median forecast with 95% CI); **inset** same data in log-lin scale. **Note**: We currently do not (yet) incorporate the uncertainties that are introduced by nowcasting, compared to using the reported cases. This leads to *over-confident* parameter estimates, including the effective spreading rate $\lambda^*(t)$; the shown uncertainties are underestimated. **C**: Comparison of total reported cases and the model (same representation as in B). **D–G**: Priors (gray lines) and posteriors (purple histograms) of all model parameters; inset values indicate the median and 95% credible intervals of the posteriors.

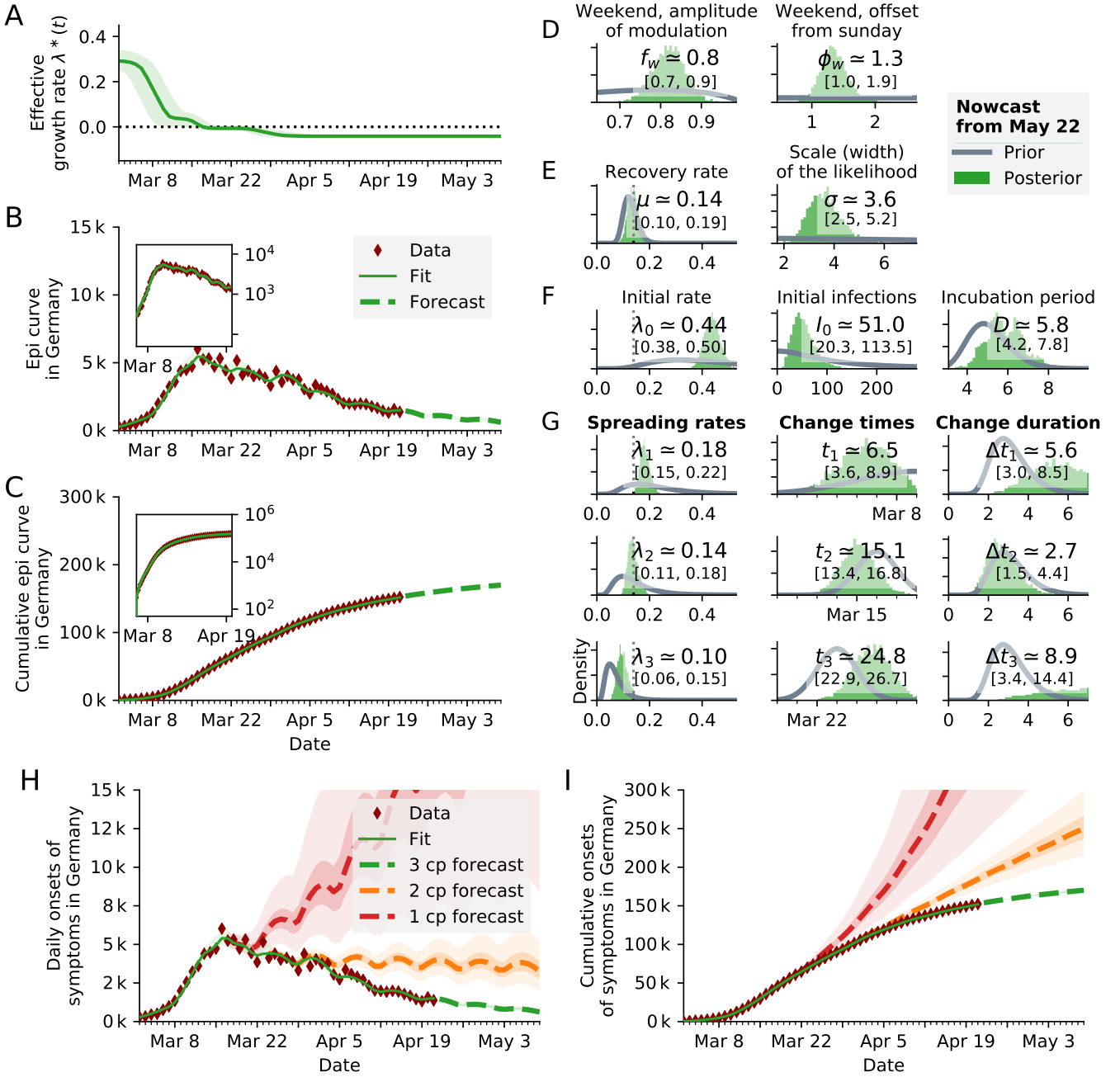


FIG. 17. **SIR model using the onset of symptoms** (unsmoothed Nowcast from May 22 [25]) of the RKI data for inference. The median of the lognormal prior of the delay between infection and onset of symptoms has been set to 5 days (right-most panel F). **A**: Time-dependent model estimate of the effective spreading rate $\lambda^*(t)$. **Note**: We currently do not (yet) incorporate the uncertainties that are introduced by nowcasting, compared to using the reported cases. This leads to *over-confident* parameter estimates, including the effective spreading rate $\lambda^*(t)$; the shown uncertainties are underestimated. **B**: Comparison of daily new reported cases and the model (green solid line for median fit with 95% credible intervals, dashed line for median forecast with 95% CI); **inset**: same data in log-lin scale. **Note**: We currently do not (yet) incorporate the uncertainties that are introduced by nowcasting, compared to using the reported cases. This leads to *over-confident* parameter estimates, including the effective spreading rate $\lambda^*(t)$; the shown uncertainties are underestimated. **C**: Comparison of total reported cases and the model (same representation as in B). **D–G**: Priors (gray lines) and posteriors (green histograms) of all model parameters; inset values indicate the median and 95% credible intervals of the posteriors. **H–I** The fitted model with two alternative forecasts. We consider in addition one scenario where only one intervention happened (red) and one where two interventions happened (orange). Includes 50% and 95% CI.

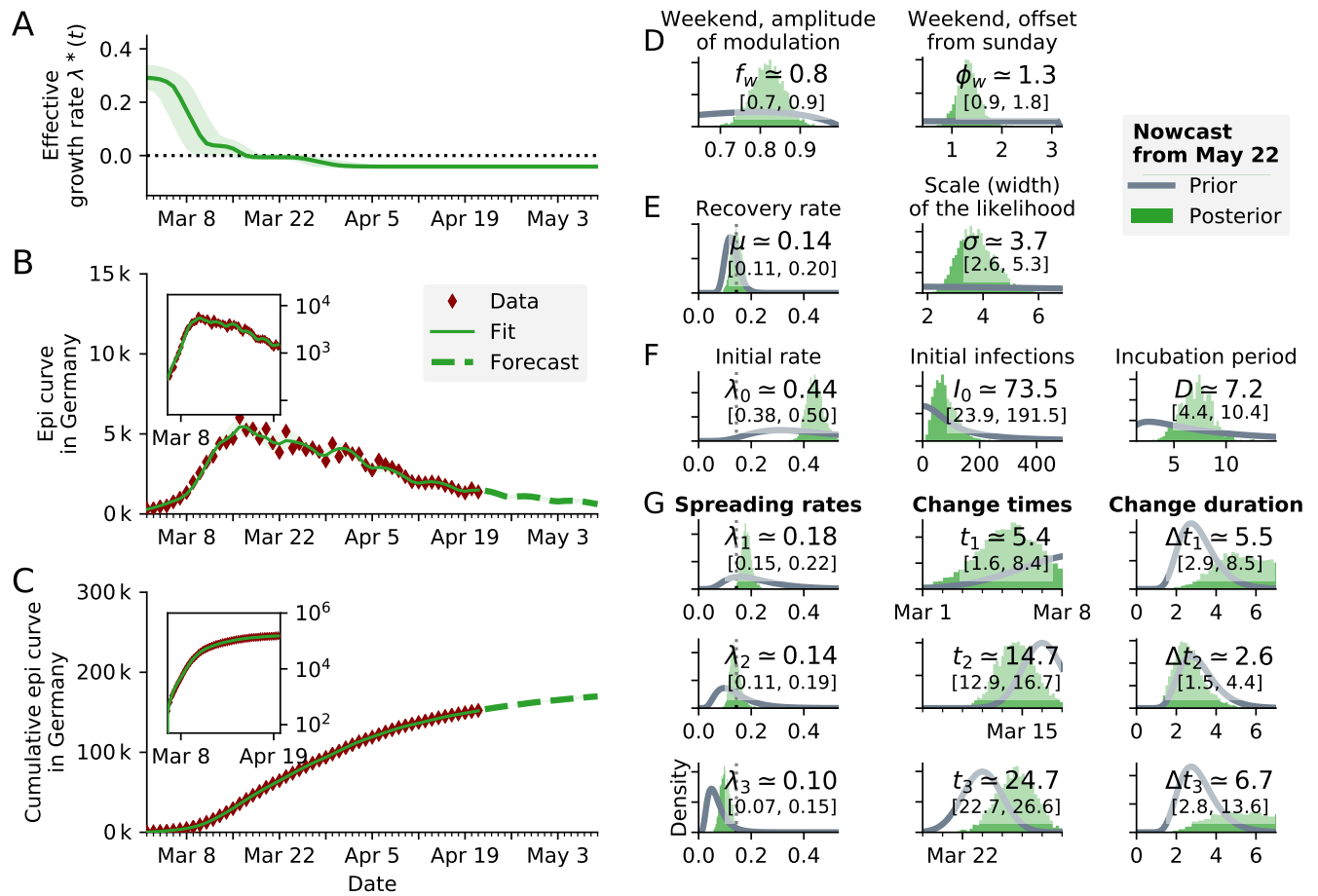


FIG. 18. SIR model using the onset of symptoms (unsmoothed Nowcast from May 22 [25]) of the RKI data for inference. The median of the lognormal prior of the delay between infection and onset of symptoms has been set to a relatively uninformative prior (right-most panel F). The posterior of the delay has as median 7.2 days, which is close to the expected incubation period of 5 days. **A**: Time-dependent model estimate of the effective spreading rate $\lambda^*(t)$. **Note**: We currently do not (yet) incorporate the uncertainties that are introduced by nowcasting, compared to using the reported cases. This leads to *over-confident* parameter estimates, including the effective spreading rate $\lambda^*(t)$; the shown uncertainties are underestimated. **B**: Comparison of daily new reported cases and the model (green solid line for median fit with 95% credible intervals, dashed line for median forecast with 95% CI); **inset** same data in log-lin scale. **C**: Comparison of total reported cases and the model (same representation as in B). **D–G**: Priors (gray lines) and posteriors (green histograms) of all model parameters; inset values indicate the median and 95% credible intervals of the posteriors.

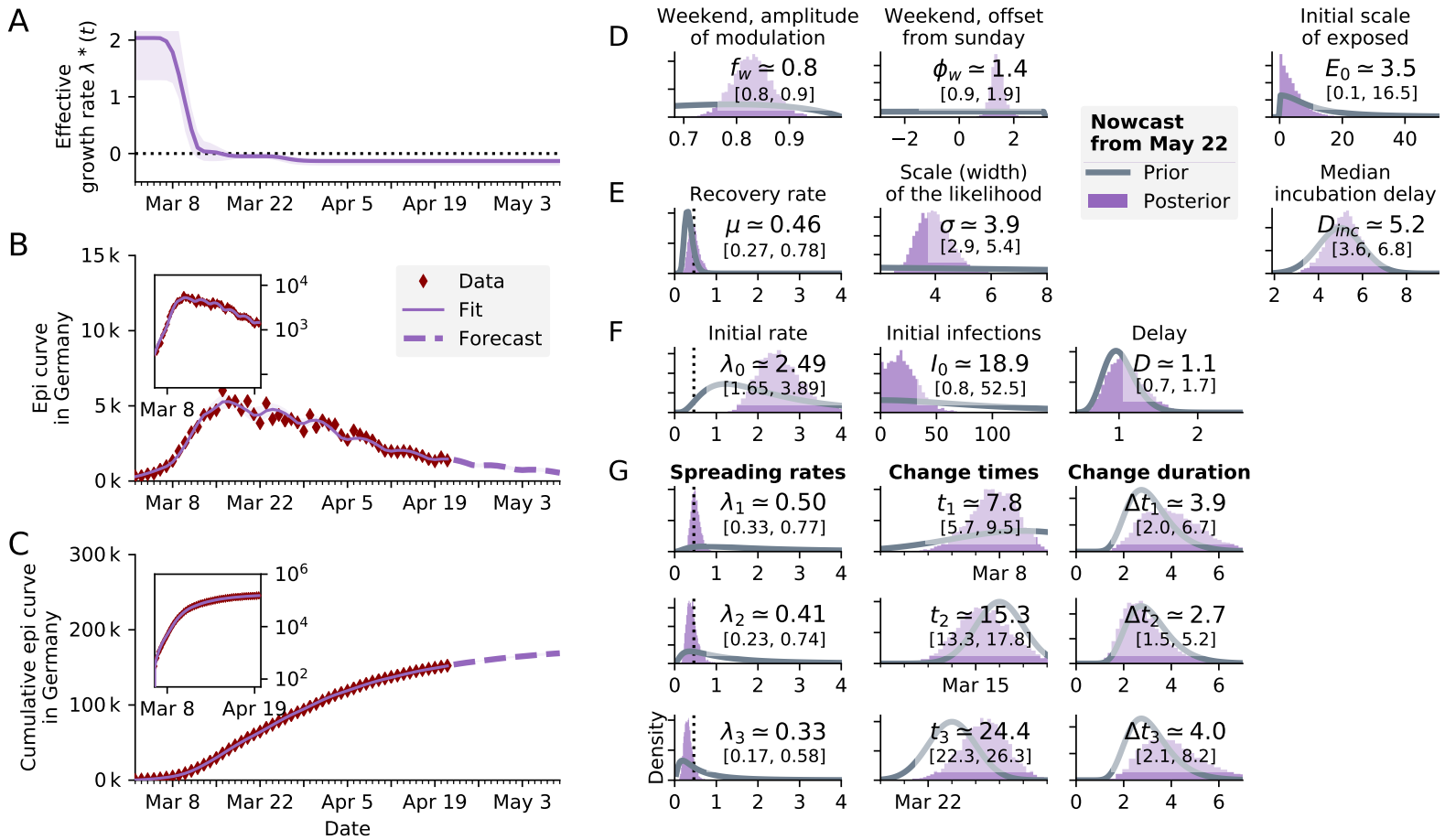


FIG. 19. **SEIR-like model using the onset of symptoms** (unsmoothed Nowcast from May 22 [25]) of the RKI data for inference. The median of the lognormal prior of the delay between infectious and onset of symptoms has been set to 1 day (right-most panel F). **A**: Time-dependent model estimate of the effective spreading rate $\lambda^*(t)$. **Note**: Due to different model dynamics, $\lambda^*(t)$ can only be compared *qualitatively* between SEIR and SIR models. The numeric values of the rates (μ , λ etc.) differ between models because they reflect the duration a person remains in a given compartment. **Note**: We currently do not (yet) incorporate the uncertainties that are introduced by nowcasting, compared to using the reported cases. This leads to *over-confident* parameter estimates, including the effective spreading rate $\lambda^*(t)$; the shown uncertainties are underestimated. **B**: Comparison of daily new reported cases and the model (purple solid line for median fit with 95% credible intervals, dashed line for median forecast with 95% CI); **inset** same data in log-lin scale. **C**: Comparison of total reported cases and the model (same representation as in B). **D–G**: Priors (gray lines) and posteriors (purple histograms) of all model parameters; inset values indicate the median and 95% credible intervals of the posteriors.

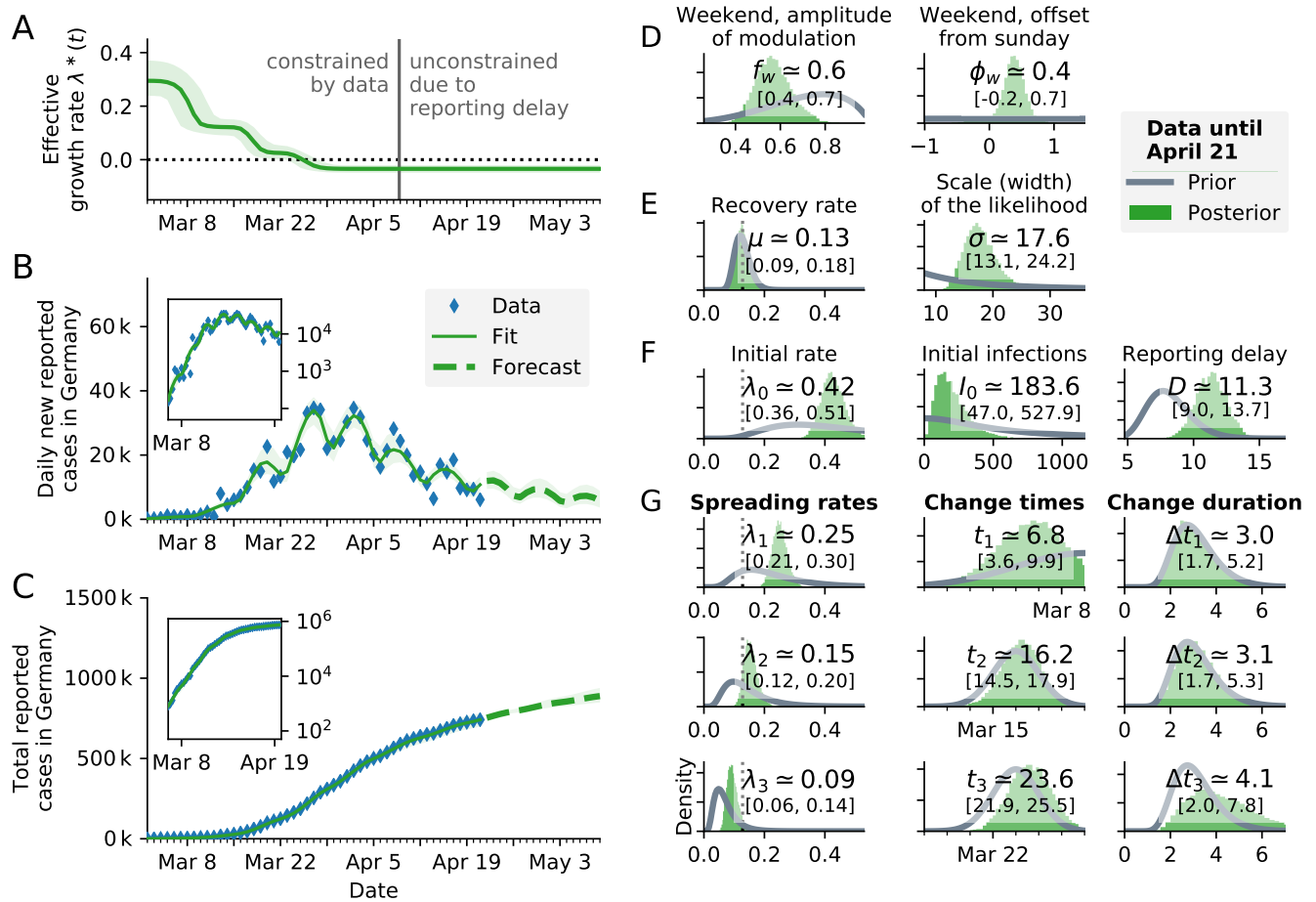


FIG. 20. SIR model **with reported case number multiplied by 5, to account for an eventual factor five of unknown cases**. Results are nearly identical to original non-multiplied plot (Fig 3. in [1]), showing that a constant underreporting has a negligible effect. The median inferred spreading rates λ are about 0.01 larger. **A**: Time-dependent model estimate of the effective spreading rate $\lambda^*(t)$. **B**: Comparison of daily new reported cases and the model (green solid line for median fit with 95% credible intervals, dashed line for median forecast with 95% CI); inset same data in log-lin scale. **C**: Comparison of total reported cases and the model (same representation as in B). **D–G**: Priors (gray lines) and posteriors (green histograms) of all model parameters; inset values indicate the median and 95% credible intervals of the posteriors.

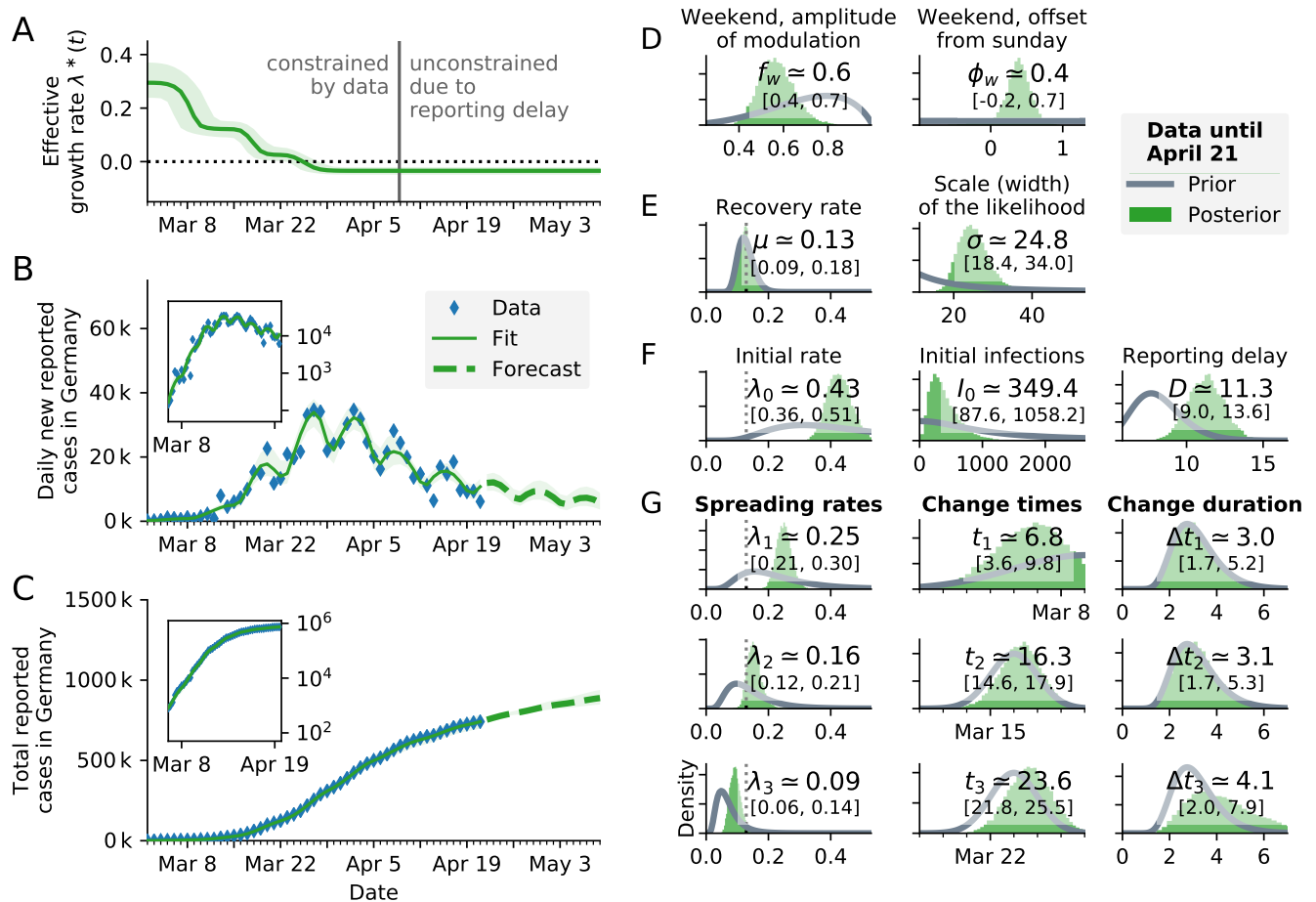


FIG. 21. SIR model **with reported case number multiplied by 10, to account for an eventual factor 10 of unknown cases**. Results are nearly identical to original non-multiplied plot (Fig 3. in [1]), showing that a constant under-reporting has a negligible effect, similar to Fig. 20. The median inferred spreading rates λ are 0.01-0.02 larger. **A**: Time-dependent model estimate of the effective spreading rate $\lambda^*(t)$. **B**: Comparison of daily new reported cases and the model (green solid line for median fit with 95% credible intervals, dashed line for median forecast with 95% CI); **inset** same data in log-lin scale. **C**: Comparison of total reported cases and the model (same representation as in B). **D–G**: Priors (gray lines) and posteriors (green histograms) of all model parameters; inset values indicate the median and 95% credible intervals of the posteriors.

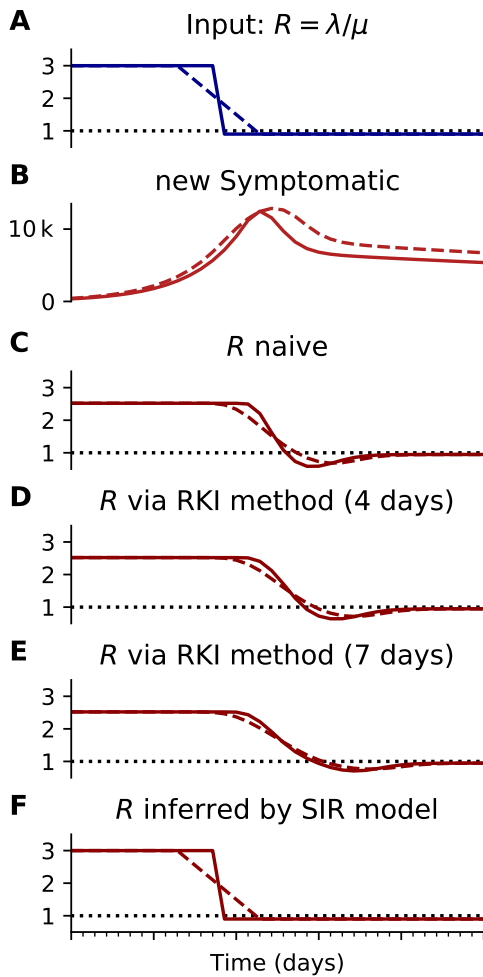


FIG. 22. Inferring R with different methods (like Fig. 4), using a synthetic model **with $R = 3$ to $R = 0.9$** . **A, B:** Synthetic data for new symptomatic cases generated with SIR dynamics from an underlying R with one change point of duration 1 day (solid) or 7 days (dashed). **C:** Model-free inference of R based on the ratio of case numbers at time t and time $t - g$. **D:** Model-free inference of R following the Robert Koch Institute convention, i.e. using the definition of C but with averaging over a window of the past 4 days. **E:** Same as D but averaging over 7 days. Note the overlap of intervals. All the model-free methods (C–E) can show an erroneous estimate of $R < 0.9$ transiently, due to the change point in the underlying true R . **F:** The inferred R using change-point detection with an underlying dynamic model (SIR) does *not* show a transient erroneous $R < 0.9$ period. If the underlying dynamic model corresponds well enough to the true disease dynamics, then this approach reproduces the true R that was used to generate the data.

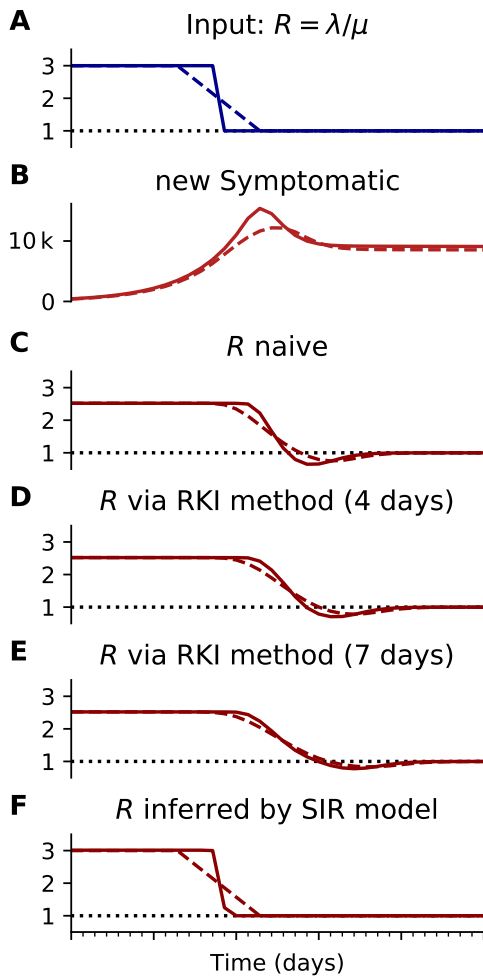


FIG. 23. Inferring R with different methods (like Fig. 4), using a synthetic model **with** $R = 3$ **to** $R = 1$. **A**, **B**: Synthetic data for new symptomatic cases generated with SIR dynamics from an underlying R with one change point of duration 1 day (solid) or 7 days (dashed). **C**: Model-free inference of R based on the ratio of case numbers at time t and time $t - g$. **D**: Model-free inference of R following the Robert Koch Institute convention, i.e. using the definition of **C** but with averaging over a window of the past 4 days. **E**: Same as **D** but averaging over 7 days. Note the overlap of intervals. All the model-free methods (**C**–**E**) can show an erroneous estimate of $R < 1$ transiently, due to the change point in the underlying true R . **F**: The inferred R using change-point detection with an underlying dynamic model (SIR) does *not* show a transient erroneous $R < 1$ period. If the underlying dynamic model corresponds well enough to the true disease dynamics, then this approach reproduces the true R that was used to generate the data.

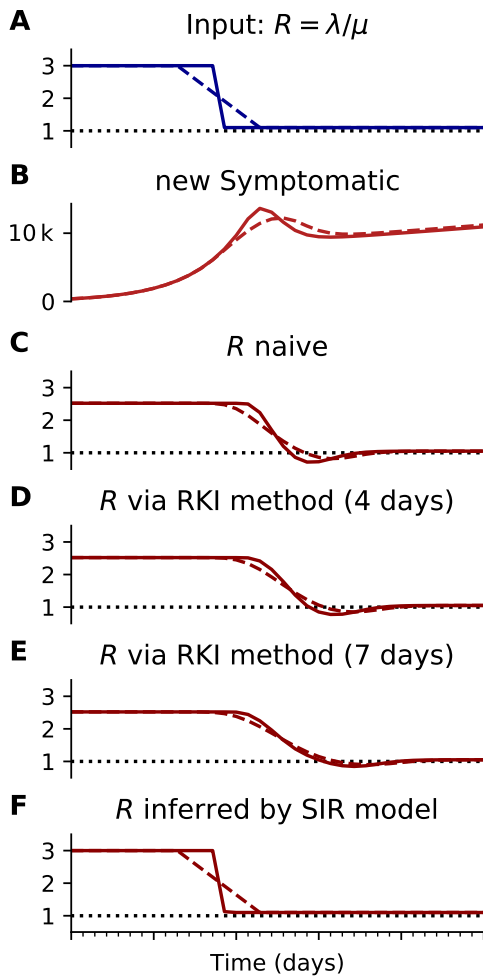


FIG. 24. Inferring R with different methods (like Fig. 4), using a synthetic model **with $R = 3$ to $R = 1.1$** . **A, B:** Synthetic data for new symptomatic cases generated with SIR dynamics from an underlying R with one change point of duration 1 day (solid) or 7 days (dashed). **C:** Model-free inference of R based on the ratio of case numbers at time t and time $t - g$. **D:** Model-free inference of R following the Robert Koch Institute convention, i.e. using the definition of C but with averaging over a window of the past 4 days. **E:** Same as D but averaging over 7 days. Note the overlap of intervals. All the model-free methods (C–E) can show an erroneous estimate of $R < 1$ transiently, due to the change point in the underlying true R . **F:** The inferred R using change-point detection with an underlying dynamic model (SIR) does *not* show a transient erroneous $R < 1$ period. If the underlying dynamic model corresponds well enough to the true disease dynamics, then this approach reproduces the true R that was used to generate the data.